

# Tectono-metamorphic evolution of a convergent back-arc: The Famatinian orogen, Sierra de Quilmes, Sierras Pampeanas, NW Argentina

Melanie A. Finch<sup>1,†</sup>, Roberto F. Weinberg<sup>1</sup>, Pavlína Hasalová<sup>2</sup>, Raul Becchio<sup>3</sup>, M. Gabriela Fuentes<sup>3</sup>, and Allen Kennedy<sup>4</sup>

<sup>1</sup>*School of Earth, Atmosphere and Environment, Monash University, Clayton, Victoria 3800, Australia*

<sup>2</sup>*Centre for Lithospheric Research, Czech Geological Survey, Klárov 3, 118 21 Prague 1, Czech Republic*

<sup>3</sup>*Instituto Geonorte, Instituto de Investigaciones en Energía no Convencional (INENCO)–Consejo Nacional de Investigaciones Científicas y Técnicas (CONICET), National University of Salta, Avenida Bolivia 5150, 4400 Salta, Argentina*

<sup>4</sup>*Department of Physics and Astronomy, Curtin University, Bentley, Western Australia 6102, Australia*

## ABSTRACT

Back-arcs are hot regions of enduring weakness in the hinterland of subduction zones that are commonly sites of strain localization, forming mobile belts that, in some cases, develop into mountain belts. Their evolution results from their strength, a function of thickness, heat flux, and stresses. Contractual back-arcs may be too weak to form thick crusts, whereas in other cases, they can thicken considerably and lead to mountain building. The stress and thermal histories of back-arcs can be retrieved from investigation of the relationships between deformation and metamorphism. The 490–430 Ma Famatinian orogen of the Sierras Pampeanas is associated with a back-arc that has a complex development. We focus on the Sierra de Quilmes within the northern section of the back-arc and present new structural data tied to anatexis and constrained by geochronology. We find that low-pressure–high-temperature conditions prevailed over an ~35 m.y. thermal peak between 497 and 461 Ma, as indicated by U/Pb ages of monazite. Anatexis coincided with thrusting to the west and northwest, as evidenced by leucosomes in axial planes of folds and in thrust planes. As rocks were thrust upward, they cooled, melt solidified, and deformation localized into two major thrust zones. These record the same thrust-to-the-west or northwest kinematics as the earlier syn-anatectic deformation and ultimately placed hot rocks over cold ones. Continuous thrusting during cooling from peak metamorphism, accompanied by strain localization, is consistent with a number of shear zones in the northern

Sierras Pampeanas. The low-pressure metamorphic assemblages indicate that shortening was not accompanied by pronounced crustal thickening, suggesting that the lithosphere was too hot, and the partially melted crust was too weak for substantial stacking.

## INTRODUCTION

During subduction, strain partitions into mobile belts in back-arcs because they are enduring sites of weakness, commonly active over several orogenic events (Katz, 1985; Hyndman et al., 2005). Their weakness is a result of high heat flux (Hyndman et al., 2005), often ascribed to lithospheric thinning due to extension in the back-arc (e.g., Wickham and Oxburgh, 1985). However, many mobile belts in back-arcs are hot despite recording crustal shortening. This could be a result of (1) inheritance of heat from an early extensional event (e.g., Loosveld and Etheridge, 1990; Forbes et al., 2008; Lister and Forster, 2009), (2) contact metamorphism with magmatic rocks (e.g., Alasino et al., 2014), or (3) upwelling of the asthenosphere below the back-arc, or increased rates of shallow convection of the asthenosphere due to the addition of volatiles from the downgoing plate, independent of whether the lithosphere was extending or shortening (Loosveld and Etheridge, 1990; Hyndman et al., 2005). The heat source may be understood in ancient back-arcs by investigating their structural and metamorphic evolution. However, the long-lived nature of mobile belts typically means that early events may be obscured by subsequent ones.

The Famatinian back-arc (490–430 Ma; Rapela et al., 1998a) in NW Argentina outcrops in a series of discontinuous mountain blocks over 1000 km along strike (between 22°S and 33°S; Coira et al., 2009). The evolution of the back-arc was complex and possibly responded to different

events along its length: Southern sections show evidence for terrane collision, but such evidence is absent north of ~26°S (Lucassen et al., 2000), in the Puna, Cordillera Oriental, and the northern Sierras Pampeanas (Fig. 1A), perhaps suggesting the collisional terrane was a ribbon that did not extend to the north. According to the literature, the northern section (the Puna and the Cordillera Oriental; Fig. 1A) underwent an early period of extension that caused deposition of thick sedimentary sequences onto the back-arc in the Early to Middle Ordovician (ca. 485–460 Ma; Bahlburg, 1990, 1991). This was followed by a period of shortening, the Oclroyic tectonic phase (450–430 Ma; Turner and Méndez, 1975; Bahlburg and Hervé, 1997; Rapela et al., 1998a), as a result of collision of the Laurentia-derived Cuyania terrane with the continental margin (Thomas and Astini, 1996; Astini and Dávila, 2004), or accelerated approach of the terrane prior to collision in the southern Sierras Pampeanas (Rapela et al., 1998a). However, in some regions in the northern Famatinian back-arc, thrust shear zones were active early in the Famatinian (e.g., the 480–424 Ma Agua Rosada shear zone, 25°S–26°S; Hongn and Riller, 2007; Wegmann et al., 2008), contemporaneous with sedimentation. The back-arc in the northern Sierras Pampeanas, Puna, and Cordillera Oriental is interpreted as a mobile belt that localized deformation related to subduction on the paleo-Pacific margin of Gondwana (Lucassen et al., 2000; Becchio and Lucassen, 2002), but our understanding of its complex development is incomplete.

This study examined a representative section of the northern back-arc exposed in the Sierra de Quilmes, focusing on the structural and thermal evolution together with geochronology. This region records crustal shortening that occurred much earlier than other sections of the back-arc (e.g., Coira et al., 2009; Hongn et al., 2014).

<sup>†</sup>melaniefinch@gmail.com

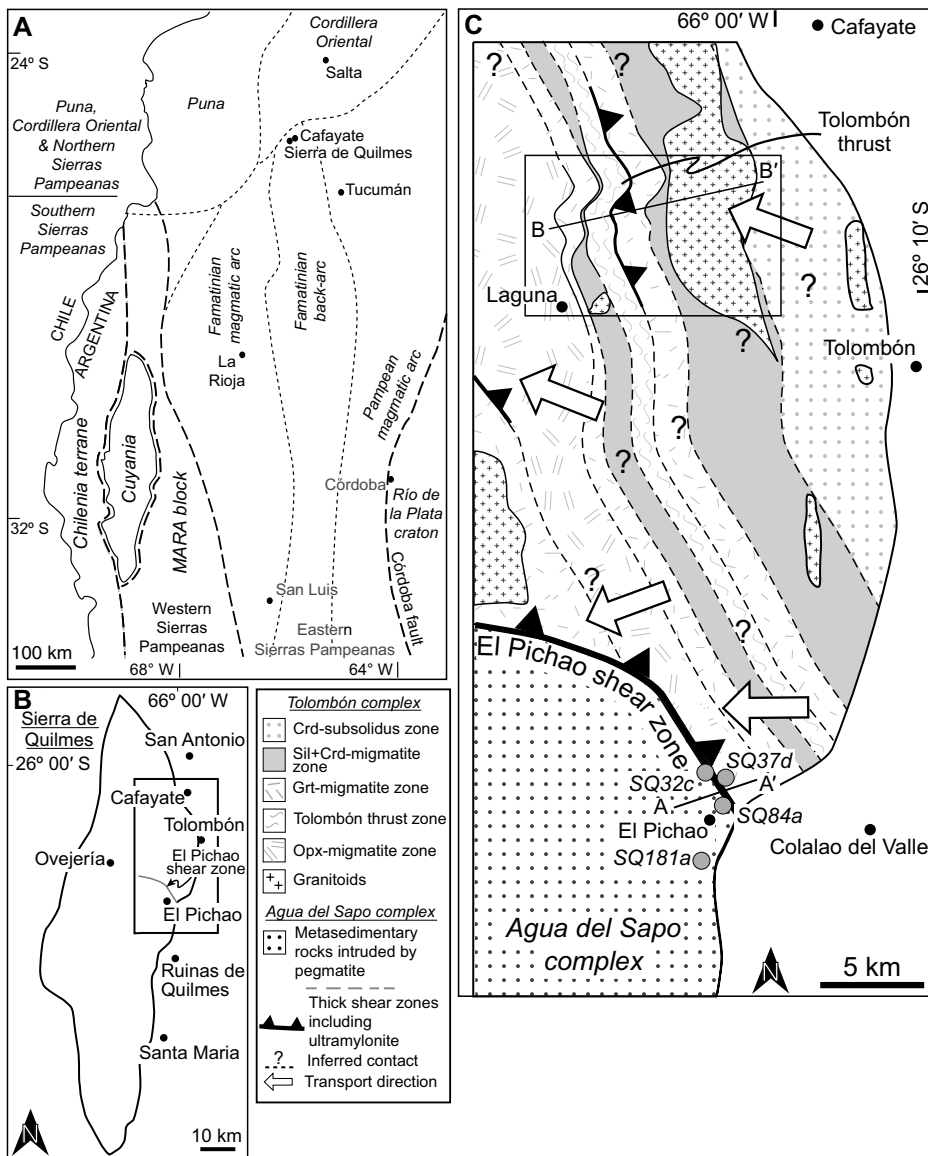


**Figure 1.** (A) Schematic outline of cratons and terranes of NW Argentina (modified from Rapela et al., 2016; Larrovere et al., 2016). (B) Outline of the Sierra de Quilmes mountain block with the region shown in C boxed. (C) Metamorphic zones of the Tolombón complex and its contact with the Agua del Sapo complex. Box corresponds to the area in Figure 2, lines A-A' and B-B' mark cross sections in Figure 3, and waypoints (gray circles) noted near the El Pichao shear zone are the locations of samples used for dating. For a detailed map of El Pichao shear zone, see Finch et al. (2015a). Crd—cordierite; Sil—sillimanite; Grt—garnet; Opx—orthopyroxene.

### GEOLOGIC SETTING

The Famatinian mobile belt consists of sedimentary rocks deposited from the late Neoproterozoic to the Early Ordovician. The more voluminous and basal sedimentary sequence is the Puncoviscana Formation, which was deposited on the southwest margin of Gondwana between 670 and 530 Ma, forming an interbedded psammite and pelite turbidite sequence (Turner, 1960; Rapela et al., 1998a).

The 550–510 Ma Pampean orogeny (Aceñolaza and Toselli, 1973) accreted the Puncoviscana Formation onto the Río de la Plata craton and caused deformation and granulite facies metamorphism in the southern Sierras Pampeanas (Rapela et al., 1998b) and low- to medium-grade metamorphism in the north (Knüver and Miller, 1981). Early Ordovician sedimentary rocks were deposited on the shallow-marine Ordovician foreland and were derived from the Famatinian volcanic arc (Bahlburg, 1991),

which was a result of the Famatinian orogeny that commenced ~20 m.y. after the end of the Pampean orogeny (Aceñolaza and Toselli, 1973). The arc is now exposed as a 200 km wide band trending N-S roughly at ~67°W (Fig. 1A; Pankhurst et al., 1998). U-Pb zircon geochronology in magmatic rocks indicates the arc was active between ca. 490 and 460 Ma, with the most voluminous activity around 470 Ma (Pankhurst et al., 1998; Bellos et al., 2015). It includes S-type granites, voluminous I-type granitic rocks at the top ranging downwards to diorites, gabbros and mafic and ultramafic cumulates, minor intrusions of tonalite-trondhjemite-granodiorite sequences (Pankhurst et al., 2000), and kilometer-wide contact aureoles (Alasino et al., 2014). East of the Famatinian arc, between 65°W and 67°W (Fig. 1A), high-temperature–low-pressure metamorphism and anatexis (Larrovere et al., 2011) and bimodal volcanism (Coira et al., 2009) characterize the back-arc zone. Thick sedimentary sequences deposited into a back-arc basin in the Early to Middle Ordovician (485–450 Ma; Bahlburg, 1990, 1991) are preserved in the Puna and the Cordillera Oriental (Fig. 1A) and include the Santa Victoria Group, which consists of shallow-water pelites and arenites (Turner, 1960; Moya, 1988). In the Puna, Early Ordovician (ca. 485–470 Ma) sedimentary packages, including the Tolar Chico, Tolillar, and Diablo formations, are overlain by the Middle to Late Ordovician (ca. 470–450 Ma) Puna turbidite complex, which contains rocks that record a progressively deeper marine setting upward, indicative of basin subsidence (Bahlburg, 1990; Zimmerman et al., 2002). The upper section of the turbidite complex contains volcaniclastic input thought to be sourced from the Famatinian volcanic arc (Zimmerman et al., 2002).

The Oclóyic tectonic phase generated pervasive mylonitic shear zones in the Sierras Pampeanas, including the Tres Arboles shear zone (Simpson et al., 2003), the Arenosa Creek shear zone (Castro de Machuca et al., 2012), the Tinogasta-Pituitil-Antinaco shear zone (Höckenreiner et al., 2003, their TIPA shear zone), and late stages of shearing on the Agua Rosada shear zone (Wegmann et al., 2008). This has led to the suggestion that the Oclóyic tectonic phase was related to shortening and closure of the Famatinian back-arc (Rapela et al., 1998a; Astini and Dávila, 2004). Once the Cuyania terrane finished colliding with the continent margin south of 29°S (Fig. 1A), the Famatinian orogeny ended (Thomas and Astini, 2003, and references therein; Varela et al., 2011).

The Sierra de Quilmes is a 140 km long mountain range located in the northern Sierras Pampeanas, west of the town Cafayate (Fig. 1;

Rossi de Toselli et al., 1976). It consists of the metamorphic equivalents of the Puncoviscana Formation, divided in two complexes according to metamorphic facies: the amphibolite facies Agua del Sapo complex in the south of the range, and the granulite facies Tolombón complex to the north (Fig. 1C; Toselli et al., 1978). The El Pichao–Ovejería shear zone thrusts the Tolombón complex over the Agua del Sapo complex. The eastern part of this shear zone, the El Pichao shear zone, is a NW-trending, 3.5 km thick mylonitic-ultramylonitic shear zone located west of the village Colalao del Valle (Figs. 1B and 1C; Finch et al., 2015a, 2016). The Ovejería section of the shear zone, to the west, is equally thick and varies between NW-trending sections that record thrusting to the west, and E–W-trending sections with a strong sinistral component, which act as transform shear zones.

The Agua del Sapo complex consists of garnet- and cordierite-bearing gneisses and schists that are intruded by pegmatite dikes (Toselli et al., 1978). The Tolombón complex is a tilted metamorphic sequence (Figs. 1–3) with increasing metamorphic grade from northeast to southwest (Büttner et al., 2005). According to Büttner et al. (2005), metamorphic grade increases from the chlorite zone to the biotite-muscovite zone, then into the garnet-cordierite-sillimanite zone, and finally into the orthopyroxene zone. Evidence for anatexis is first apparent in their biotite-muscovite zone, with muscovite-dehydration melting reactions. Evidence for biotite-dehydration melting is found in the higher grade zones (Büttner et al., 2005). Migmatites are mainly stromatic metatexites, with diatexites more common in the higher grade zones in the southwest (Figs. 2 and 3). To the east of the complex, the composite Cafayate pluton intruded into sillimanite-cordierite migmatites (Rapela and Shaw, 1979).

Büttner et al. (2005) dated migmatites from the Tolombón complex and found that monazite growth occurred between 485 and 450 Ma (range incorporates uncertainties on ages from U/Pb thermal ionization mass spectrometry [TIMS] dating), better constraining earlier Rb–Sr ages (Rapela et al., 1982; Miller et al., 1991). Lucassen et al. (2000) dated garnet from a deformed gneiss from Anchillo gorge (in the Tolombón complex and immediate hanging wall of the El Pichao shear zone) to  $442 \pm 9$  Ma (Sm–Nd mineral isochrons). The data of Büttner et al. (2005) suggest a high-temperature regime between 485 and 450 Ma, with cooling through muscovite closure by ca. 442 Ma (Ar–Ar). Using the mean of the high-temperature age range, Büttner et al. (2005) suggested peak metamorphism occurred at 470 Ma and

was accompanied by ductile shearing, which continued as cooling proceeded to amphibolite facies and localized to major shear zones (Finch et al., 2015a). Ductile shearing ended with the thrusting of migmatites onto lower grade rocks (Finch et al., 2015a), which Büttner et al. (2005) suggested was at ca. 440 Ma based on the age of undeformed pegmatites that crosscut ductile shear zones.

Büttner (2009) described a zone of intense shearing in the Tolombón complex, separating the biotite-muscovite zone in the hanging wall from the garnet-cordierite-sillimanite zone in the footwall. He interpreted this as a detachment that allowed the lower grade rocks to deform differently than the migmatites. He estimated the paleopressure of key samples in the migmatitic terrane using multi-equilibrium methods and found that the current distance between samples was less than the vertical distance that should separate them based on pressure determinations. From this, he inferred that the package as a whole had been thinned, indicating crustal extension. Büttner (2009) recognized that the shear sense throughout the Sierra de Quilmes is top-to-the-W and top-to-the-NW thrusting, and suggested that the shear zones were originally horizontal, accommodating crustal extension, and rotated to their current dip during the Andean orogeny.

Finch et al. (2015a) studied the El Pichao shear zone, where the granulite facies migmatites of the Tolombón complex are on the hanging wall, above lower grade rocks of the Agua del Sapo complex. They interpreted this hot-over-cold sequence as a result of the regional top-to-the-W and top-to-the-NW thrusting, indicating shortening rather than extension. Büttner (2015) argued that Finch et al. (2015a) did not date movement on the El Pichao shear zone and were therefore unable to relate movement on the El Pichao shear zone to shearing in the rest of the Tolombón complex, and that thrusting of the high-grade package could have occurred after peak metamorphism and extension. However, Finch et al., (2015a, 2015b) argued that the amphibolite facies El Pichao shear zone recorded the same kinematics as that recorded during anatexis in the migmatites, suggesting continuity of thrusting. In this paper, we expand on this argument by introducing new data and return to this question in the discussion. An integral part of this controversy is an understanding of the nature of the heat source in the Sierra de Quilmes. If peak metamorphism occurred during extensional shearing, the high heat flux was likely a result of lithospheric thinning. However, if the region was under shortening for most of its history, another heating mechanism could have been involved in generating the voluminous magmatic products.

## ANALYTICAL METHODS

Mineral compositions were analyzed using the HyperProbe field-emission gun electron probe microanalyzer at the Microbeam Laboratory at the Commonwealth Scientific and Industrial Research Organisation (CSIRO) in Clayton, Victoria, Australia, in point beam mode and the Tescan Vega scanning electron microscope equipped with an X-Max 50 energy-dispersive (EDS) detector at Charles University in Prague, Czech Republic. Mineral compositions are listed in Table 1, and mineral abbreviations are after Kretz (1983).

Samples for geochronology were crushed and milled, and monazite was separated using magnetic and heavy liquids separation techniques. Grains of a variety of appearances were handpicked under a binocular microscope and mounted on a 25 mm epoxy disk along with the monazite standard IND-1 (509 Ma,  $^{206}\text{Pb}/^{238}\text{U} = 0.082133$ ; Korhonen et al., 2011). The mount was polished, and prior to analysis, all monazite grains were photographed in transmitted light; after gold coating, samples were imaged using backscattered electron (BSE images) microscopy on the scanning electron microscope, which revealed that grains did not exhibit any zoning (so images are not presented here). Monazites are rounded to irregular, light yellow in color and vary in size from ~100 to 1000  $\mu\text{m}$ . Monazites were dated using the sensitive high-resolution ion microprobe (SHRIMP)–II at the John de Laeter Centre at Curtin University in Western Australia. The procedure for monazite dating followed the method described in Korhonen et al. (2011). For each sample, three grains were re-analyzed at the end of the run using a different spot to ensure accuracy was maintained over the run. Common Pb was corrected using  $^{204}\text{Pb}$ , after  $^{204}\text{Pb}$  was corrected for the interference correlation with Th concentration (Stern and Berman, 2001). The mean ages were weighted, and the error shown for each mean age incorporates the error in the standard (Table 2).

Selected trace and rare earth element concentrations of monazites were determined via laser-ablation–inductively coupled plasma–mass spectrometry (LA-ICP-MS). The mount used was the same from the SHRIMP geochronology, polished to remove the gold coating. The analyses were carried out using a New Wave UP 213 nm N:YAG laser-ablation microprobe coupled with a Thermo Finnigan X series II quadrupole ICP-MS at Monash University's School of Earth, Atmosphere and Environment. Analyses were in helium atmosphere, employing a pulse rate of 5 Hz and beam energy of ~8 J/cm<sup>2</sup> at the sample and laser spot size of 30  $\mu\text{m}$  diameter. For each analysis, background readings were

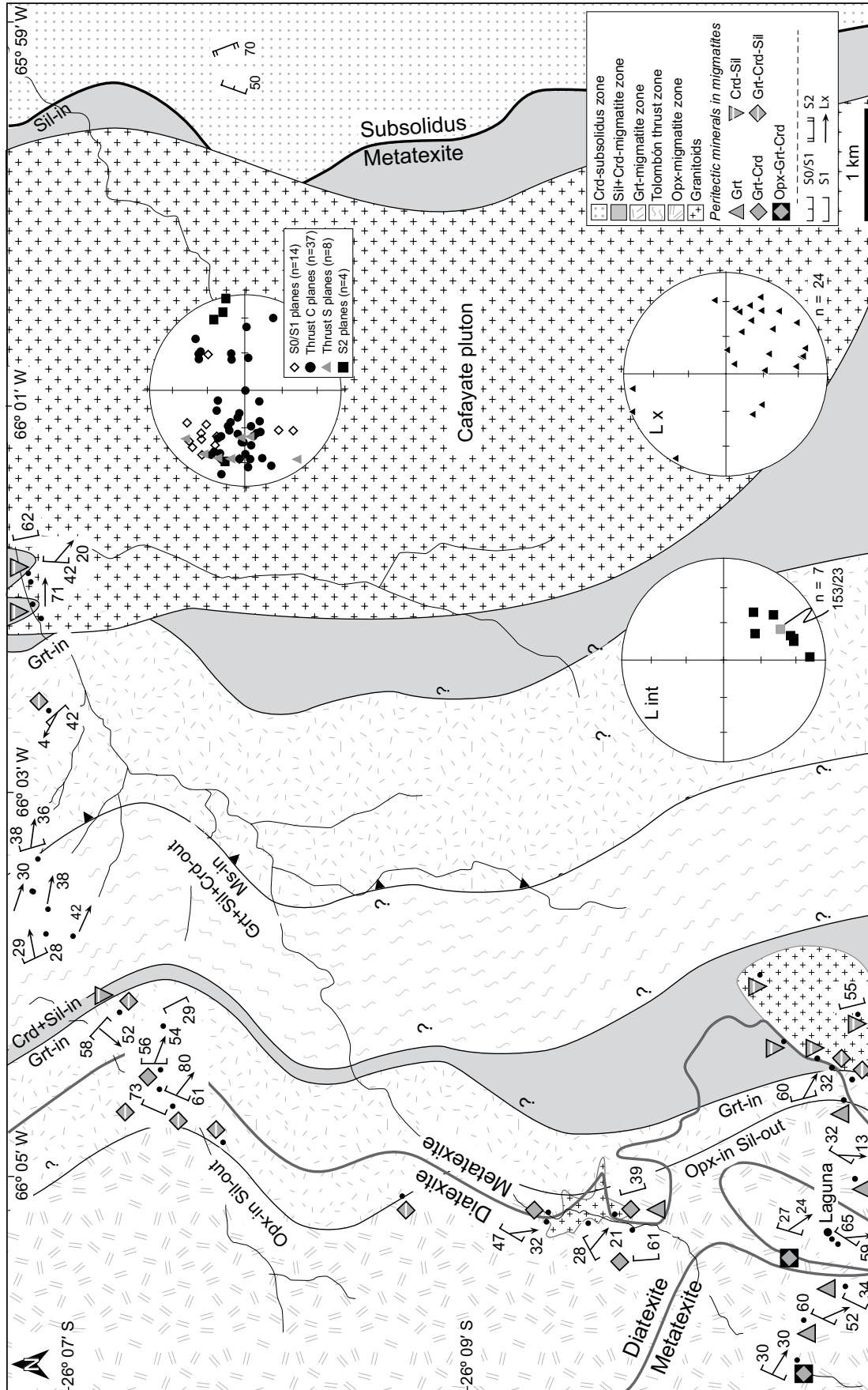
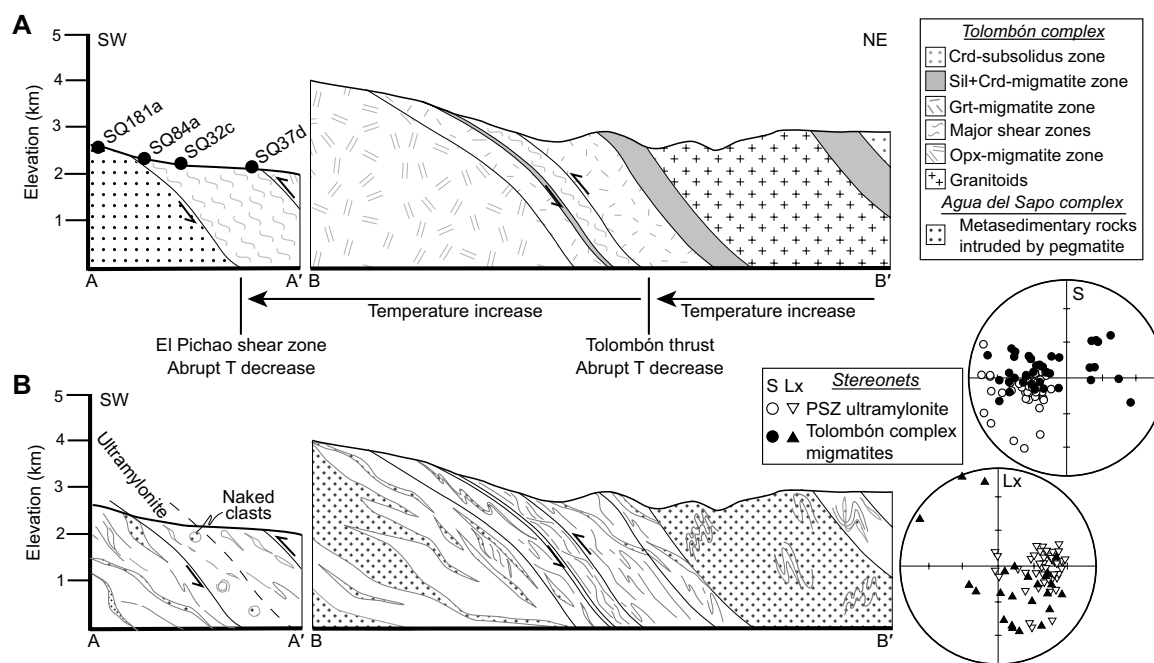


Figure 2. Geological map of the metamorphic zones defined in this study. See Figure 1C for location. Black circles are waypoints and indicate outcrop locations. Contacts extrapolated beyond waypoints were interpreted from Google Earth imagery and Figure 2 in Büttner et al. (2005). Bold black lines indicate change in leucosome proportion (subsolidus, metatexite, diatexite). Diatexites are separated into different metamorphic zones on the basis of mineralogy. Inset: Stereonets for poles to foliations (top), intersection lineation (L int, left), and stretching lineation (Lx, right) for all zones. Stereonets are lower-hemisphere, equal-area projections. Mineral abbreviations are after Kretz (1983).



**Figure 3.** (A) Schematic cross section of the Tolombón complex showing repetition of metamorphic zones by thrust zones and locations of samples for geochronology. (B) Schematic representation of structures and their intensity in the metamorphic zones of the Tolombón complex. The line of the section is shown in Figure 1C. Insets: Stereonets comparing orientations of C-planes (S) and stretching lineations (Lx) for mylonitic rocks of the El Pichao shear zone (PSZ; Finch et al., 2015a) and deformed rocks of the Tolombón complex between Laguna and Cafayate (Fig. 2). Crd—cordierite; Sil—sillimanite; Grt—garnet; Opx—orthopyroxene.

collected for 30 s, followed by 60 s ablation time. The LA-ICP-MS raw data were reduced using the GLITTER 4.0 software package (Van Achterbergh et al., 2001), and quantitative results for the trace elements were obtained using NIST610 glass as a primary external standard and U.S. Geological Survey (USGS) BHVO 2G as a secondary standard. Ca concentrations of monazite obtained from Büttner et al. (2005, see the electronic supplement) were used for internal standardization. The USGS standard BCR 2G was analyzed throughout the analytical session to check for precision and accuracy.

**METAMORPHISM IN THE TOLOMBÓN COMPLEX**

In this section, we use the term migmatite to describe any rocks that have been partially melted, metatexite for migmatites that retain their original coherence and typically have stromatic layering, diatexite for rocks that have lost coherence due to high melt fraction, leucosome for the crystallized product of the melt, and melanosome for the solid or residual part of the rock left behind after melt was extracted (Sawyer, 2008). The melanosome usually has a high concentration of biotite, commonly accompanied by peritectic minerals.

**Metamorphic Zones in the Tolombón Complex**

We describe metamorphic rocks from a region that extends 20 km west into the mountain range between the town of Cafayate and the village of Colalao del Valle (Fig. 1C). Similar to Büttner et al. (2005), we observed metamorphic zones that are marked by the appearance of index minerals. We defined six zones oriented approximately NNW-SSE that generally increase in metamorphic conditions to the west, except when this trend is broken due to repetition caused by shear zones (Figs. 2 and 3). The zones are: (1) biotite + chlorite (Bt + Chl) zone, (2) cordierite (Crd)–subsolidus zone, (3) sillimanite + cordierite (Sil + Crd)–migmatite zone, (4) garnet (Grt)–migmatite zone, (5) Tolombón thrust zone, and (6) orthopyroxene (Opx)–migmatite zone. These are simplified zone names based on their most significant minerals (zones 1–4 and 6).

**Bt + Chl Zone**

Low-grade metasedimentary rocks are exposed north and east of San Antonio (Fig. 1B). They comprise two interbedded lithologies: pelite forms brown to green layers, and psammite forms brown to gray layers. Pelite layers

contain Qtz + Chl + Ilm + Bt + Ms + Kfs + Pl, and psammite layers contain Qtz + Kfs + Pl + Bt + Chl + lithic fragments. These rocks retain primary structures such as cross-bedding, Bouma sequences, and compositional layering (Büttner et al., 2005). A bedding-parallel cleavage, S1, is defined by aligned micas and is more pronounced in pelitic layers. These rocks are intruded by Ms + Tur ± Grt pegmatite and tonalitic and two-mica granitic dikes that are parallel to bedding. The base of this zone has not been identified in the field area of this study, but it is defined by the absence of chlorite, broken down to form biotite and muscovite (Büttner et al., 2005).

**Crd-Subsolidus Zone**

This zone consists of a >1.5 km thick section characterized by the disappearance of chlorite and the appearance of Crd in the absence of leucosomes (Fig. 4A). Like the Bt + Chl zone, these rocks are intruded by granitic dikes (Fig. 4B). Magma intrusion is more voluminous in pelitic layers, where it occasionally disaggregates the country rock. In these regions, pelite rafts and biotite-rich schlieren are evident within “dirty” granites, which form mappable units. Table 1 summarizes the mineralogy for this and all other zones described herein.

TABLE 1. SUMMARY OF MINERAL APPEARANCES IN THE TOLOMBÓN COMPLEX

	Sil	Crd	Grt	Opx	Ms	Pl	Kfs	Qtz	Bt	Accessories
<b>Crd-subsolidus zone</b>										
<b>Metapelites</b>		10%; <2 cm, poikiloblastic			5%	15%; <0.1 mm	<5%; <0.1 mm	15%; <0.1 mm	45%; <0.5 mm; mica fish or flakes, Zrn radiation damage haloes	Zrn, Ap, Mnz, Ilm
<b>Metapsammities</b>					5%	15%; <1 mm	5%; <1 mm	65%; <1 mm; bulging and undulose extinction	10%; <1 mm	Zrn, Ap, Mnz
<b>Sil+Crd-migmatite zone (leucosome = 10%–20% of rock)</b>										
<b>Leucosome</b>	<10%; fibrous, individual grains or layers	<5%; <3 mm; retrogressed to plinite or replaced by Ms			<5%; small, sparse grains	15%; lamellar crystallization twins; forms myrmekite around Kfs; cusped, indented grain boundaries	10%; tartan twinning; cusped, indented grain boundaries	50%; chessboard extinction; cusped, indented grain boundaries	<5%; small, sparse grains	
<b>Melanosome</b>	10%; layers and aggregates <5 mm length; fibrolite and blocky crystals adjacent to Bt	Up to 75%; partially replaced by Sil+Bt			<5%; <3 mm flakes; euhedral; overgrow Bt with Ilm+Rt	<5%	<5%	<5%	Up to 85%; <3 mm; Zrn radiation haloes; partially replaced by Sil+Ilm+Rt or Ms+Ilm+Rt, or Chl	Qtz, Pl, Kfs, Chl, Ilm, Rt
<b>Grt-migmatite zone (leucosome = 30% of rock)</b>										
<b>Leucosome</b>	<2%; occasional thin continuous bands	10%; <3 mm, occurs in aggregates <5 cm diameter; retrogressed to plinite or Sil; $X_{Fe} = 0.38$			2%; small, sparse grains	10%; lamellar crystallization twins; forms myrmekite around Kfs	15%; tartan twinning and perthitic	50%; chessboard extinction	<5%; small, sparse grains; $X_{Fe} = 0.55$	
<b>Melanosome</b>	2%; replaces Crd	Up to 75%; partially replaced by Sil+Bt	5%–10%; increasing size to west; <3 cm; partially replaced by Bt; Alm <sub>77</sub> , Prp <sub>14</sub> , Sp <sub>56</sub> , Grs <sub>5</sub>			<5%	<5%	<5%	Up to 70%; <1 mm long; partially replaced by Ilm+Ms+Rt	Qtz, Pl, Kfs, Ilm, Rt, Sp, Mag
<b>Opx-migmatite zone (leucosome = 30%–70% of rock)</b>										
<b>Leucosome</b>		5%–10%; <2 cm; inclusions of Zrn, Bt, Qtz; partially replaced by Bt; $X_{Fe} = 0.32$	5%–15%; <3 cm; poikiloblastic with inclusions of Qtz & wormy Ilm; partially replaced at edges by Bt and Chl; Alm <sub>67</sub> , Prp <sub>23</sub> , Sp <sub>56</sub> , Grs <sub>3</sub>	5%; pleochroic; <3 cm, inclusions of Grt; replaced by Grt, Bt+Ilm or Bt+Qtz intergrowths; $X_{Fe} = 0.55$		10%; lamellar crystallization twins; forms myrmekite around Kfs	15%; tartan twinning and perthitic	60%; chessboard extinction	<5%; small, sparse grains; $X_{Fe} = 0.51$	
<b>Melanosome</b>	2%; replaces Crd	Up to 75%; partially replaced by Sil+Bt	5%–10%; partially replaced by Bt	<5%		<5%	<5%	<5%	Up to 70%; <2 mm flakes adjacent to leucosomes; thin layers parallel to foliation	Qtz, Pl, Kfs, Ilm, Rt, Sp, Ky, Mag, Opx

Note: The first value in percentage is modal content of each individual mineral. Almandine (Alm) = Fe/(Ca + Fe + Mg + Mn), spessartine (Sps) = Mn/(Ca + Fe + Mg + Mn), pyrope (Prp) = Mg/(Ca + Fe + Mg + Mn),  $X_{Fe} = Fe/(Fe + Mg)$ . Mineral abbreviations are after Kretz (1983).

TABLE 2. U/Pb ANALYTICAL DATA

Sample	Spot name	U (ppm)	Th (ppm)	Th/U	Radiogenic ratios								Age (Ma) <sup>206</sup> Pb/ <sup>238</sup> U	Discord. %
					<sup>207</sup> Pb/ <sup>235</sup> U	±%	<sup>206</sup> Pb/ <sup>238</sup> U	±%	<sup>238</sup> U/ <sup>206</sup> Pb	±%	<sup>207</sup> Pb/ <sup>206</sup> Pb	±%		
<u>Mylonite from El Pichao shear zone after stromatic metatexite</u>														
SQ37d	37.1	3951	43,253	11	0.621	1.3	0.0798	1.1	12.53	1.1	0.05642	0.78	495 ± 5	-6
<i>n</i> = 25	37.2	7346	39,783	5	0.590	1.3	0.0764	1.1	13.09	1.1	0.05597	0.64	475 ± 5	-6
	37.3	2533	38,833	15	0.616	1.3	0.0785	1.1	12.74	1.1	0.05690	0.69	487 ± 5	-0
	37.4	5334	43,594	8	0.598	1.7	0.0766	1.7	13.05	1.7	0.05660	0.46	476 ± 8	-1
	37.5	3534	44,492	13	0.588	1.4	0.0754	1.2	13.25	1.2	0.05650	0.62	469 ± 5	+0
	37.6	4094	47,642	12	0.614	1.2	0.0784	1.1	12.76	1.1	0.05684	0.51	487 ± 5	-1
	37.7	2973	45,934	15	0.596	2.2	0.0761	2.1	13.13	2.1	0.05674	0.67	473 ± 9	+1
	37.8	2809	46,166	16	0.597	1.3	0.0772	1.1	12.96	1.1	0.05616	0.72	479 ± 5	-5
	37.9	2867	46,349	16	0.596	1.9	0.0765	1.8	13.07	1.8	0.05650	0.64	475 ± 8	-1
	37.11	4228	42,598	10	0.592	1.8	0.0758	1.8	13.20	1.8	0.05664	0.54	471 ± 8	+1
	37.12	2763	56,726	21	0.584	1.3	0.0746	1.1	13.40	1.1	0.05679	0.71	464 ± 5	+4
	37.13	3654	42,813	12	0.593	1.3	0.0768	1.2	13.02	1.2	0.05601	0.59	477 ± 5	-6
	37.14	1277	50,887	40	0.603	1.8	0.0789	1.1	12.67	1.1	0.05545	1.40	490 ± 5*	-15
	37.15	3412	47,232	14	0.582	1.4	0.0765	1.2	13.07	1.2	0.05513	0.67	475 ± 5*	-15
	37.16	6054	48,305	8	0.570	1.7	0.0738	1.7	13.54	1.7	0.05602	0.49	459 ± 7	-2
	37.17	4025	43,115	11	0.602	1.2	0.0781	1.1	12.81	1.1	0.05594	0.58	485 ± 5	-9
	37.18	3659	32,798	9	0.614	1.6	0.0796	1.4	12.56	1.4	0.05598	0.64	494 ± 7	-10
	37.19	1289	57,095	44	0.606	2.3	0.0768	2.1	13.01	2.1	0.05724	0.97	477 ± 10	+4
	37.21	656	53,718	82	0.596	2.2	0.0776	1.2	12.89	1.2	0.05576	1.84	482 ± 6	-10
	37.22	2161	45,386	21	0.583	1.6	0.0747	1.3	13.39	1.3	0.05659	0.89	464 ± 6	+2
	37.23	5319	45,340	9	0.592	1.4	0.0764	1.3	13.08	1.3	0.05621	0.49	475 ± 6	-4
	37.24	2165	50,640	23	0.585	1.5	0.0756	1.3	13.22	1.3	0.05606	0.82	470 ± 6	-4
	37.1R	4733	37,937	8	0.593	1.8	0.0762	1.8	13.13	1.8	0.05642	0.47	473 ± 8	-2
	37.19R	1030	56,717	55	0.599	2.0	0.0774	1.5	12.91	1.5	0.05612	1.33	481 ± 7	-6
	37.23R	4218	52,617	12	0.596	1.3	0.0772	1.1	12.95	1.1	0.05597	0.61	479 ± 5	-7
	Weighted mean												477 ± 5	
<u>Ultramylonite from El Pichao shear zone after granitic diatexite</u>														
SQ32c	32.1	1667	33,252	20	0.576	2.4	0.0763	2.0	13.11	2.0	0.05477	1.17	474 ± 9*	-19
<i>n</i> = 17	32.2	2199	34,395	16	0.614	1.6	0.0809	1.3	12.36	1.3	0.05501	0.91	501 ± 6*	-23
	32.5	1887	35,004	19	0.589	1.6	0.0760	1.3	13.15	1.3	0.05617	0.92	472 ± 6	-4
	32.6	1981	36,910	19	0.626	1.4	0.0816	1.1	12.26	1.1	0.05568	0.82	505 ± 6*	-16
	32.7	894	35,083	39	0.588	2.9	0.0789	1.2	12.67	1.2	0.05401	2.58	490 ± 6*	-34
	32.8	941	34,190	36	0.566	4.2	0.0754	2.9	13.26	2.9	0.05442	3.01	469 ± 13*	-22
	32.11	4920	47,649	10	0.643	1.2	0.0815	1.1	12.27	1.1	0.05724	0.46	505 ± 5	-1
	32.3	3705	30,874	8	0.617	1.3	0.0788	1.2	12.70	1.2	0.05679	0.58	489 ± 6	-2
	32.4	1461	35,661	24	0.618	1.7	0.0782	1.4	12.79	1.4	0.05731	0.90	485 ± 7	+3
	32.12	832	35,607	43	0.632	2.1	0.0769	1.6	13.01	1.6	0.05961	1.38	477 ± 7*	+19
	32.13	1037	34,095	33	0.527	3.7	0.0740	3.0	13.52	3.0	0.05171	2.18	460 ± 13*	-73
	32.14	2055	33,884	16	0.560	2.4	0.0730	2.2	13.69	2.2	0.05567	0.81	454 ± 10	-4
	32.15	1389	34,529	25	0.577	2.2	0.0754	1.9	13.27	1.9	0.05556	1.12	468 ± 9	-9
	32.16	2460	32,169	13	0.500	2.0	0.0688	1.5	14.53	1.5	0.05263	1.22	429 ± 6*	-39
	32.7R	1046	36,912	35	0.589	1.9	0.0758	1.5	13.19	1.5	0.05629	1.20	471 ± 7	-2
	32.9R	2508	33,401	13	0.558	1.4	0.0736	1.1	13.58	1.1	0.05500	0.88	458 ± 5*	-12
	32.1R	937	36,120	39	0.574	2.1	0.0754	1.5	13.25	1.5	0.05522	1.47	469 ± 7*	-12
	Weighted mean												483 ± 15	
<u>Mylonitic garnet-schist from El Pichao shear zone</u>														
SQ84a	84.1	2888	34,317	12	0.607	1.3	0.0781	1.1	12.81	1.1	0.05637	0.73	485 ± 5	-4
<i>n</i> = 14	84.2	2292	37,066	16	0.596	1.7	0.0784	1.1	12.75	1.1	0.05517	1.31	487 ± 5*	-17
	84.3	2414	37,160	15	0.579	1.8	0.0748	1.7	13.37	1.7	0.05614	0.72	465 ± 8	-2
	84.4	2155	32,214	15	0.589	2.0	0.0742	1.9	13.48	1.9	0.05755	0.73	461 ± 8	+10
	84.5	3630	39,369	11	0.570	1.5	0.0741	1.2	13.50	1.2	0.05583	0.75	461 ± 6	-4
	84.7	2310	29,184	13	0.605	1.4	0.0780	1.1	12.83	1.1	0.05629	0.77	484 ± 5	-5
	84.8	2235	37,562	17	0.576	1.5	0.0750	1.3	13.33	1.3	0.05565	0.78	466 ± 6	-7
	84.9	2086	35,404	17	0.583	1.6	0.0777	1.1	12.87	1.1	0.05442	1.16	482 ± 5*	-26
	84.10	4375	31,347	7	0.566	1.5	0.0734	1.4	13.63	1.4	0.05598	0.53	457 ± 6	-2
	84.11	2873	33,094	12	0.605	1.3	0.0778	1.1	12.86	1.1	0.05644	0.67	483 ± 5	-3
	84.13	1927	37,240	19	0.609	1.4	0.0785	1.1	12.75	1.1	0.05630	0.88	487 ± 5	-6
	84.2R	2170	35,617	16	0.567	1.5	0.0743	1.3	13.45	1.3	0.05534	0.90	462 ± 6	-9
	84.9R	2095	36,082	17	0.587	1.5	0.0749	1.3	13.35	1.3	0.05687	0.71	466 ± 6	+4
	84.7R	2359	32,528	14	0.586	1.4	0.0755	1.3	13.24	1.3	0.05625	0.70	470 ± 6	-2
	Weighted mean												472 ± 7	
<u>Muscovite-garnet schist from Agua del Sapo complex</u>														
SQ181a	181.1	4920	26,203	6	14.29	1.1	0.05570	0.49	0.537	1.2	0.0700	1.1	436 ± 5	+1
<i>n</i> = 15	181.2	4621	27,999	6	14.38	1.1	0.05561	0.52	0.533	1.2	0.0695	1.1	433 ± 5	+0
	181.3	3843	20,208	5	14.64	1.2	0.05445	0.78	0.513	1.4	0.0683	1.2	426 ± 5	-10
	181.4	3103	30,649	10	14.99	1.5	0.05501	0.80	0.506	1.7	0.0667	1.5	416 ± 6	-1
	181.5	3557	23,526	7	15.01	1.5	0.05536	0.68	0.509	1.6	0.0666	1.5	416 ± 6	+2
	181.6	3881	28,225	8	14.74	1.2	0.05496	0.73	0.514	1.4	0.0678	1.2	423 ± 5	-4
	181.7	3147	19,565	6	14.93	1.2	0.05625	0.66	0.519	1.4	0.0670	1.2	418 ± 5	+9
	181.8	4583	26,434	6	14.47	1.1	0.05493	0.60	0.523	1.2	0.0691	1.1	431 ± 5	-6
	181.9	2428	29,437	13	14.04	1.1	0.05513	0.82	0.541	1.4	0.0712	1.1	443 ± 5	-7
	181.10	3954	11,996	3	14.32	1.2	0.05479	0.69	0.527	1.4	0.0698	1.2	435 ± 5	-9
	181.11	4781	23,851	5	14.65	1.4	0.05528	0.57	0.520	1.5	0.0682	1.4	426 ± 6	-1
	181.12	5265	26,722	5	14.96	1.6	0.05545	0.54	0.511	1.6	0.0669	1.6	417 ± 6	+3
	181.1R	4767	27,913	6	14.38	1.1	0.05492	0.61	0.527	1.3	0.0696	1.1	433 ± 5	-7
	181.3R	3422	10,409	3	14.69	1.2	0.05525	0.68	0.518	1.4	0.0681	1.2	424 ± 5	-1
	181.7R	4847	27,588	6	15.05	1.6	0.05523	0.56	0.506	1.7	0.0664	1.6	415 ± 7	+1
	Weighted mean												428 ± 5	

Note: Common Pb was corrected using <sup>204</sup>Pb, after <sup>204</sup>Pb was corrected for the interference correlation with Th concentration (Stern and Berman, 2001). All errors on ages are 2σ. Discord.—discordance.

\*Age >10% discordant and not included in the weighted mean calculation.

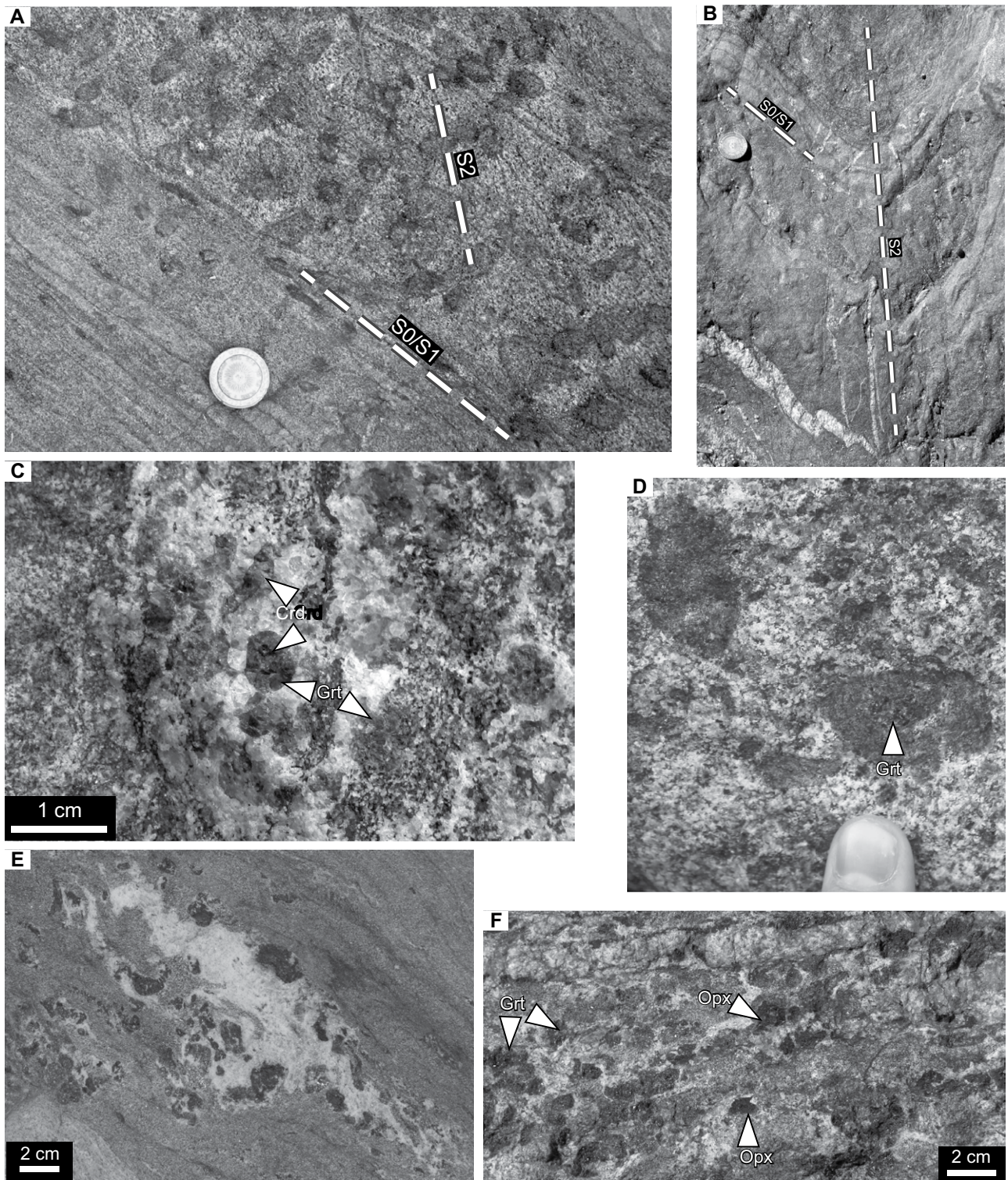


Figure 4. Typical features of rocks of the Tolombón complex. (A) Contact between psammite and pelite layers in cordierite-subsolidus zone. Pelitic layers contain porphyroblasts of cordierite and two well-developed dissolution cleavages, S1 and S2. S1 is parallel to S0 and is also seen in psammite layers. (B) Upright F2 fold in psammo-pelite in cordierite-subsolidus zone. S0 and S1 are folded, and S2 is a dissolution cleavage that defines the axial plane. Thin granitic dikes are parallel to S0/S1 and link to the axial plane of the fold. (C) Cordierite (Crd) with garnet (Grt) corona in pelitic layer in garnet-migmatite zone. (D) Cordierite diatexite with 3-cm-long porphyroblasts of garnet (arrow) surrounded by cordierite now partly retrogressed to biotite in the garnet-migmatite zone. (E) Patchy leucosome with orthopyroxene in psammite layer from the orthopyroxene-migmatite zone. (F) Stromatic metatexite with garnet + orthopyroxene (Opx) leucosome from the orthopyroxene-migmatite zone. Photographs in A and E are parallel to stretching lineation; B is perpendicular to S2 and to the fold axis.

### *Sil + Crd–Migmatite Zone*

This 4 km thick zone is structurally below the rocks of the Crd-subsolidus zone, and it is marked by the first appearance of leucosomes (1–5 cm wide) and the first appearance of fibrous sillimanite (Figs. 5A and 5B). Typically, leucosomes comprise 10%–20% of the rock and are mostly parallel to S0/S1. Beyond sillimanite, they contain occasional grains of cordierite, and sparse grains of muscovite (Fig. 5A). These migmatites are intruded by leucogranites, which are differentiated from *in situ* leucosomes by the absence of sillimanite and melanocratic selvages, as well as their greater width (up to 50 cm; Fig. 6A). Melanosomes comprise most of the rock and are rich in Bt + Sil + Ms. Occasional films of Pl + Qtz appear on the edges of biotite grains close to leucosomes. When replacing biotite, muscovite forms a corona around Ilm + Rt, or the three minerals are intergrown (Fig. 5B).

The NE-SW-trending, 4 km wide Cafayate pluton (Rapela, 1976; Rapela and Shaw, 1979; Büttner et al., 2005) intrudes this zone and grades from leucogranite to leucotonalite across strike toward the west (Rapela and Shaw, 1979). The eastern contact is marked by an increase in the proportion of intrusions until metasedimentary rocks form rafts up to a meter long. The western contact with the Sil + Crd migmatites is sharp, and layer-parallel sills intrude the migmatite.

### *Grt–Migmatite Zone*

The first appearance of garnet signals the beginning of this ~1.5 km thick zone. In comparison to the previous zone, the proportion of cordierite increases, sillimanite and muscovite decrease, and metatexites have a higher proportion of leucosomes (~30% of the rock). Pelitic layers contain foliation-parallel leucosomes, whereas those in psammitic layers crosscut the weakly developed foliation and form patches. While garnet is mostly restricted to leucosomes, cordierite appears in both melanosomes and leucosomes (Figs. 4C, 4D, and 5C). Occasionally garnet leucosomes contain only one kind of feldspar, that is, they comprise either Kfs + Qtz + Grt or Pl + Qtz + Grt.

Melanosomes contain Bt + Sil, and green spinel appears for the first time (Table 1). Biotite and quartz intergrowths occur on the edges of leucosomes at the expense of K-feldspar. Like previous zones, this zone is intruded by granitic dikes that show sharp to diffuse boundaries with the stromatic metatexite.

Toward the west, the proportion of melt increases, and metatexites transition into diatexites over 300 m (Fig. 2). This is the first oc-

currence of diatexites, and several outcrops preserve evidence of melt segregation and extraction (Figs. 6B–6F). In this zone, melanosomes generally associated with diatexites can be very rich in peritectic minerals, with some layers or pockets with >80% Crd, Crd + Bt, or Crd + Grt + Bt (Figs. 6E and 6F), with grains surrounded by thin leucosomes interpreted to be residual melt-derived material. Restitic layers are meter-wide and can comprise up to 5% of the total outcrop (Figs. 6E and 6F).

### *Tolombón Thrust Zone*

The gradual westward increase in metamorphic conditions is interrupted by a 1.5 km thick zone marked by mylonitic rocks that thrust the Grt-migmatite zone over cooler rocks of the Sil + Crd–migmatite zone. These mylonites contain Qtz (30%) + Bt (30%) + Pl (20%) + Ms (15%) and accessory Ap, Mnz, and Fe- and Ti-oxides. They are finely banded Bt + Ms schists that are strongly sheared with top-to-the-west thrust shear sense, named here the Tolombón thrust. Within the intensely foliated, recrystallized, micaceous matrix (Figs. 5D and 5E), there are bands of Pl ± Qtz up to 1.5 cm wide where plagioclase shows simple concentric zoning sometimes truncated by the sheared matrix. Typical markers of *in situ* melting present in other zones, such as peritectic minerals, biotite and quartz intergrowths, and melanosomes with a high proportion of restitic minerals, are absent from this zone.

In the footwall of this thrust, the Sil + Crd–migmatite forms a 200-m-thick zone followed by a return to the Grt-migmatite zone (Fig. 2). Compared to the same zone in the hanging wall, the footwall Sil + Crd–migmatite zone shows an increase in sillimanite, and thin Sil + Crd-bearing leucosomes appear. The Grt-migmatite zone is ~1 km thick and becomes diatexitic toward the west, until the first appearance of orthopyroxene signals the beginning of the Opx-migmatite zone.

### *Opx–Migmatite Zone*

This >3 km thick zone is characterized by the appearance of orthopyroxene and disappearance of sillimanite from leucosomes (Table 1). Metatexites generally consist of 30%–50% leucosome and lose coherence at >50% leucosome, forming diatexites. Peritectic minerals are larger and comprise a higher proportion of the rock than in the previous zone. Orthopyroxene is more common in leucosomes in psammitic layers (Figs. 4E and 5F), cordierite in pelitic layers, and garnet is common in both (Fig. 4F; see further detail in Table 1). As in the Grt-migmatite zone, here there are leucosomes that

contain only one feldspar, either Kfs + Qtz + Grt or Pl + Qtz + Grt. Leucosomes have melanocratic selvages comprising coarse flakes of biotite, two to three times larger than in the surroundings.

Kyanite appears in melanosomes for the first time here and forms small, subhedral porphyroblasts that are randomly oriented with respect to the foliation. As in previous zones, there are occasional melanocratic layers that contain >80% residual minerals in different combinations, including Bt + Sil, Crd + Bt ± Opx, Grt + Bt ± Opx, or Grt + Crd + Bt ± Opx. Occasionally, over a distance of a few meters, there are restitic rocks with different modal contents (e.g., Grt + Bt restite meters away from Crd + Opx + Bt restite).

Within this zone, there are voluminous layers of garnet diatexite containing Qtz + Kfs + Pl + Bt + Grt ± Ms ± Chl ± Sil ± Ap with schollen of garnet-bearing psammitic and pelitic. The proportion of leucosome varies between 70% and 90% and contains tabular feldspar up to 3 cm in length. Garnet in diatexites is up to 1 cm diameter, of a similar composition to the Grt-migmatite zone (almandine; Table 1), and widely spaced, suggesting it is peritectic.

## **Summary and Interpretation of Metamorphic Zones**

The Tolombón complex exposes a tilted high-temperature–low-pressure metamorphic terrane with a gradual westward increase in metamorphic grade from greenschist to granulite facies. Büttner et al. (2005) suggested that cordierite in the Crd-subsolidus zone was a result of contact metamorphism with the Cafayate pluton and defined this zone as a Bt + Ms zone. The pluton is emplaced structurally below, within the Sil + Crd-migmatite zone, and it is difficult to distinguish whether cordierite is a result of regional or contact metamorphism. The presence of Crd + Bt + Ms and disappearance of chlorite in the Sil + Crd–migmatite zone indicate upper greenschist facies conditions (Powell and Holland, 1990). Melting starts in the Sil + Crd–migmatite zone, and the gradual increase in metamorphic grade into the Grt-migmatite zone is interrupted by the Tolombón thrust, which repeats part of the sequence. The plagioclase zoning within this thrust may be igneous or metamorphic (Vernon, 2004), and its truncation indicates zoning occurred prior to deformation. The absence of K-feldspar and high proportion of plagioclase suggest this rock may have been a tonalite, similar to rocks in the western section of the Cafayate pluton. However, the intensity of the deformation makes petrogenesis uncertain.

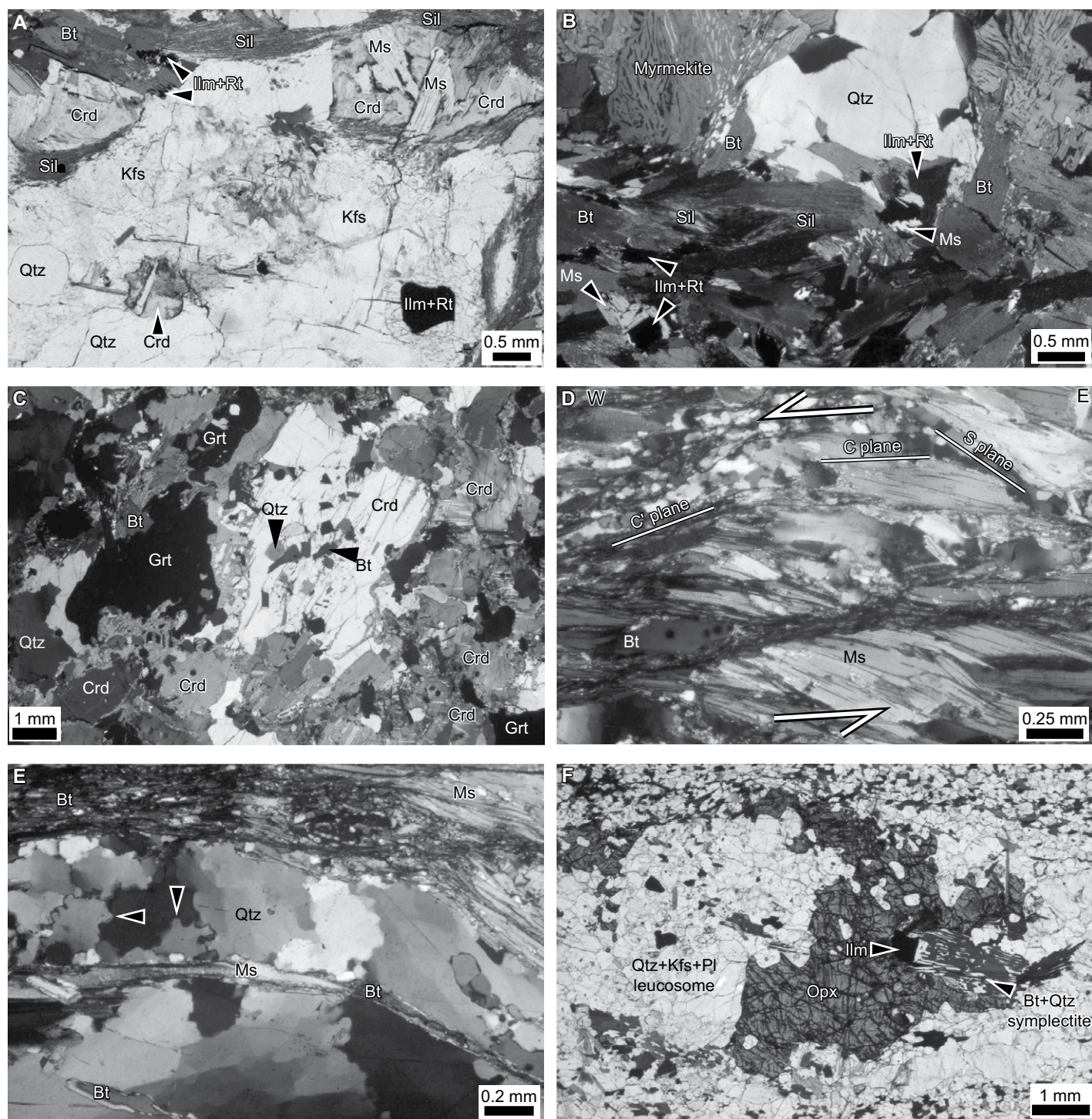


**Figure 5.** Photomicrographs showing relationships between metamorphic minerals in the Tolombón complex. (A) Leucosome from the Sil + Crd-migmatite zone. Biotite is partially replaced by Ilm + Rt, and cordierite is partially replaced by Ms + Sil. (B) Leucosome from the Sil + Crd-migmatite zone that contains myrmekite close to the boundary with melanosome. Muscovite forms coronas around Ilm + Rt, and they replace biotite. (C) Restitic rock from the Grt-migmatite zone with >80% cordierite, partially retrogressed at edges to biotite and sillimanite. Restite also contains occasional porphyroblasts of garnet and remnant biotite. (D–E) Microstructures of the Tolombón thrust zone: (D) flakes of muscovite define S-C fabric, and very fine-grained layers of Bt + Qtz + Fsp define C' planes indicating top-to-the-W shear sense; and (E) quartz in monomineralic layer shows bulging recrystallization (arrows) and chessboard extinction. (F) Orthopyroxene-bearing leucosome from the Opx-migmatite zone. Edges of orthopyroxene grain have reacted with melt to form Bt + Qtz symplectite. All thin sections are oriented parallel to stretching lineation and perpendicular to foliation. Images in A and F are plane-polarized light; images in B–E are cross-polarized light.

## STRUCTURAL GEOLOGY

### Structural Features

In the subsolidus zones (Fig. 1), two main metamorphic foliations are well developed in pelitic layers: a bedding-parallel foliation S1, and a crosscutting foliation S2 (Fig. 4A). S1 is defined by the alignment of micas and dissolution cleavage and dips moderately SE (Figs. 4A and 4B). S2 is defined by dissolution cleavage (Figs. 4A and 4B) and dips steeply west or occasionally moderately east (Figs. 2 and 4A). S2 can be traced into folded regions, where it is the axial plane of F2 folds (Figs. 2 and 4B). Folds are upright and isoclinal to open, with fold axes that plunge gently SSE, subparallel to the intersection lineation between S0/S1 and S2 (Fig. 2). No overprinting relationships between folds of different geometries were observed. Grt-Tur leucogranite intrusions are dominantly foliation-parallel in pelitic layers and crosscut or pool underneath and above psammitic layers.

Down sequence to the west, the migmatites in the Sil + Crd-migmatite zone show centimeter-scale ptygmatic folds, S-C fabric, leucosomes sheared into  $\sigma$ -clasts, and meter-scale, upright folds in the same orientation as subsolidus rocks. Leucosomes are parallel to the main foliation (S0/S1) and are linked continuously with leucosomes on the axial planes of folds (S2), which cut through fold hinges (Fig. 7). Toward the west of this zone, there are fewer folds, and asymmetrical structures become more pervasive (Fig. 3B). Migmatitic zones contain W- or NW-verging asymmetrical folds, S-C-C' fabric defined by biotite-rich planes, feldspar  $\sigma$ -clasts, showing core-mantle structure with myrmekite on foliation-parallel edges, and

The dominant melt-producing reactions in the anatectic zones of the Tolombón complex change from NE to SW. In the Sil + Crd-migmatite zone, the relatively large modal proportion of sillimanite indicates the Ms-dehydration melting reaction was dominant. Sparse grains of muscovite in leucosomes are euhedral, suggesting they are either igneous or a result of retrogression. The minor presence of cordierite (Fig. 5A) and films of Pl + Qtz on edges of biotite grains indicate incipient dehydration melting of biotite, although cordierite could also represent metamorphic cordierite grains. These features suggest melting occurred at pressures below 6 kbar and temperatures above 650 °C (Green, 1976; Vielzeuf and Holloway, 1988). In the Grt-migmatite zone, the presence of Kfs  $\pm$  Crd  $\pm$  Grt  $\pm$  Sil indicates Bt- and Ms-dehydration melting reactions (Vielzeuf and Holloway, 1988; Vielzeuf and Montel, 1994) and temperatures of >650 °C (Büttner et al., 2005). As for the Sil + Crd-migmatite zone, muscovite in this zone is sparse and euhedral, suggesting it is a result of retrogression. The disappearance of Sil in the Opx-migmatite zone indicates melting occurred dominantly through Bt dehydration (Vielzeuf and Holloway, 1988; Vielzeuf and Montel, 1994), suggesting granulite facies conditions, with temperatures above 750–850 °C and pressures ~5.5–6.5 kbar (Büttner et al., 2005).

In the migmatitic zones, biotite and quartz intergrowths on the edges of leucosomes indicate retrogression due to reaction with crystallizing melt (Kriegsman, 2001). The appearance of coarse flakes of biotite in melanosomes may have been caused by water infiltration from the crystallizing leucosome, which may have also prevented the retrogression of peritectic minerals in leucosomes (Kriegsman, 2001; White and Powell, 2010). In the Opx-migmatite zone, the replacement of orthopyroxene by garnet (Table 1) suggests a reduction in the stable modal content of orthopyroxene late in the metamorphic history. The random orientation of retrograde kyanite in this zone indicates that deformation ceased before the stability field of kyanite was reached, as interpreted by Büttner et al. (2005).

The high proportion of restitic rocks in all migmatitic zones implies significant melt removal (Figs. 6B–6F). The presence of leucosomes with only one type of feldspar suggests magma fractionation, with the Kfs leucosomes perhaps representing the mobile fraction and Pl leucosomes representing cumulates of early-formed minerals (Sawyer, 1998). This suggests not only that migmatites and leucosomes were open systems.

quartz ribbons that show grain boundary migration recrystallization and chessboard extinction (in Grt-migmatite and Opx-migmatite zones only). The stretching lineations in all zones are E- or SE-plunging (Fig. 2), defined by elongate grains of biotite, feldspar, and quartz.

Rocks in the Tolombón thrust are mylonites with well-developed  $\sigma$ -clasts, mica fish, and S-C-C' fabric defined by thin planes (<0.1 mm) of fine-grained, recrystallized quartz, biotite, feldspar, and muscovite (Fig. 5D). The geometry and kinematic indicators of this shear zone are similar to those in the hanging wall and foot-wall, but they are more intensely developed here. Quartz ribbons show bulging recrystallization or chessboard extinction (Fig. 5E, arrows) and thin or pinch out on C' planes (Fig. 5D). Bands and  $\sigma$ -shaped porphyroclasts of Pl  $\pm$  Qtz have strain shadows containing Qtz  $\pm$  Pl  $\pm$  Ms  $\pm$  Bt.

Locally within the Opx-migmatite zone, there are lithons marked by a steepening of C planes to ~60°E, concomitant with a decrease in foliation intensity (Fig. 8). These areas show only S-C fabric, whereas the surrounding regions with shallower dips have S-C-C' fabric, recumbent, west-verging isoclinal folds, leucosomes sheared into  $\sigma$ -clasts, as well as a higher proportion of leucosome and granitic dikes (Fig. 8). In more extreme and rare cases found in diatexites, leucocratic sections show little deformation and have a massive appearance, while higher strain is recorded in melanocratic areas. Other lithons in the Opx-migmatite zone (e.g., at 26°10'46.70"S, 66°05'20.40"W) contain thrust shear planes that dip W, opposite to the general trend, with a NW-plunging stretching lineation.

In the southern part of the Tolombón complex, the Opx-migmatite zone is overprinted by the 3.5 km thick El Pichao shear zone (Fig. 1),



**Figure 6 (on following page).** Examples of magma intrusion, segregation, and extraction. (A) Intrusive cordierite-bearing granite sill with sharp to diffuse contacts against a stromatic migmatite. Surrounding stromatic migmatite has in situ melt pods and leucosome layers with diffuse boundaries with melanosome. (B) Homogeneous gray granitic rock, representing magma extracted from leucosomes in metatexite, akin to dewatering features in sedimentary rocks. (C) In situ segregation of leucosome disrupting a layered pelite-psammitic block on left-hand side. Leucosome is rich in garnet and cordierite and is associated with an irregular residual region on the right-hand-side, which is rich in peritectic garnet and cordierite, and which lacks layering. (D) Stromatic migmatite. Pelitic layers have aggregates of garnet + cordierite + biotite up to 10 cm long in a leucocratic matrix and surround a psammitic layer with little peritectic minerals or leucosomes. This suggests that the pelitic layers were more fertile, and melt was extracted, leaving the residue behind. (E) Residual layer rich in garnet + biotite + cordierite surrounded by leucosome-rich bands. (F) Residual layer rich in cordierite + biotite forming a band in the center of the photograph, surrounded by bands richer in leucosome and large peritectic garnet. Note narrow leucosome network through residual layer surrounding aggregates of cordierite + biotite and directly linked with leucosome-rich areas above and below. These are interpreted to represent extraction pathways of interstitial melts.

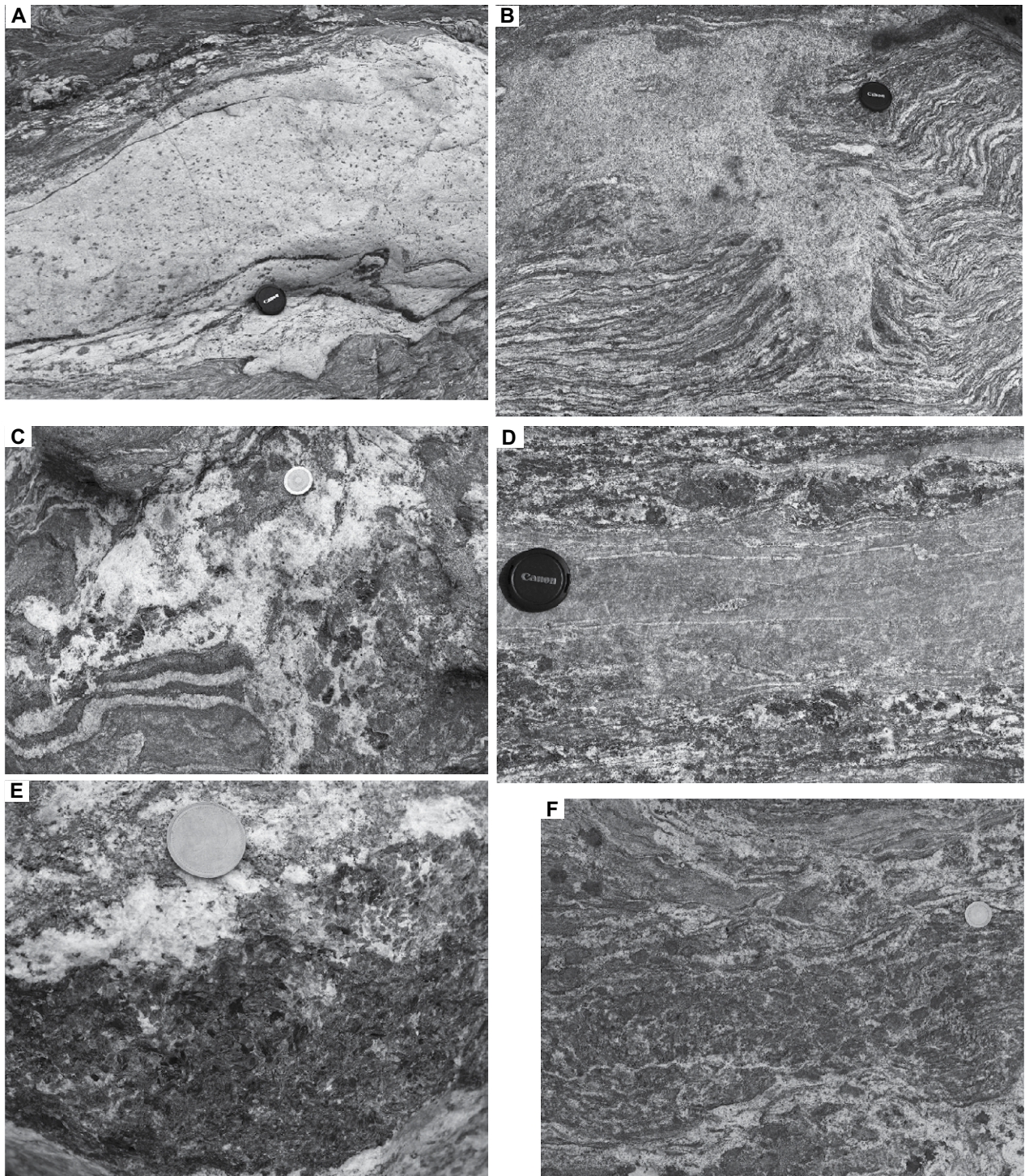


**Figure 6.**

detailed in Finch et al. (2015a). The significant aspect of the El Pichao shear zone relevant here is that it has the same kinematics as those recorded in the Tolombón complex (Fig. 3) and thrusts the granulite facies migmatites to the west onto amphibolite facies metasedimentary rocks of the Agua del Sapo complex.

**Summary and Interpretation of Structural Data**

The structures change with metamorphic grade defining two domains. The transition between the two structural domains takes place within the Sil + Crd–migmatite zone. Structur-

ally above this zone, subsolidus rocks have upright folds, whereas below this zone, migmatites are dominated by structures indicative of simple shearing, showing pervasive S-C-C' fabric, W- and NW-verging asymmetric folds, and  $\sigma$ -shaped leucosomes, reflecting thrusting to the W or NW (Fig. 3).

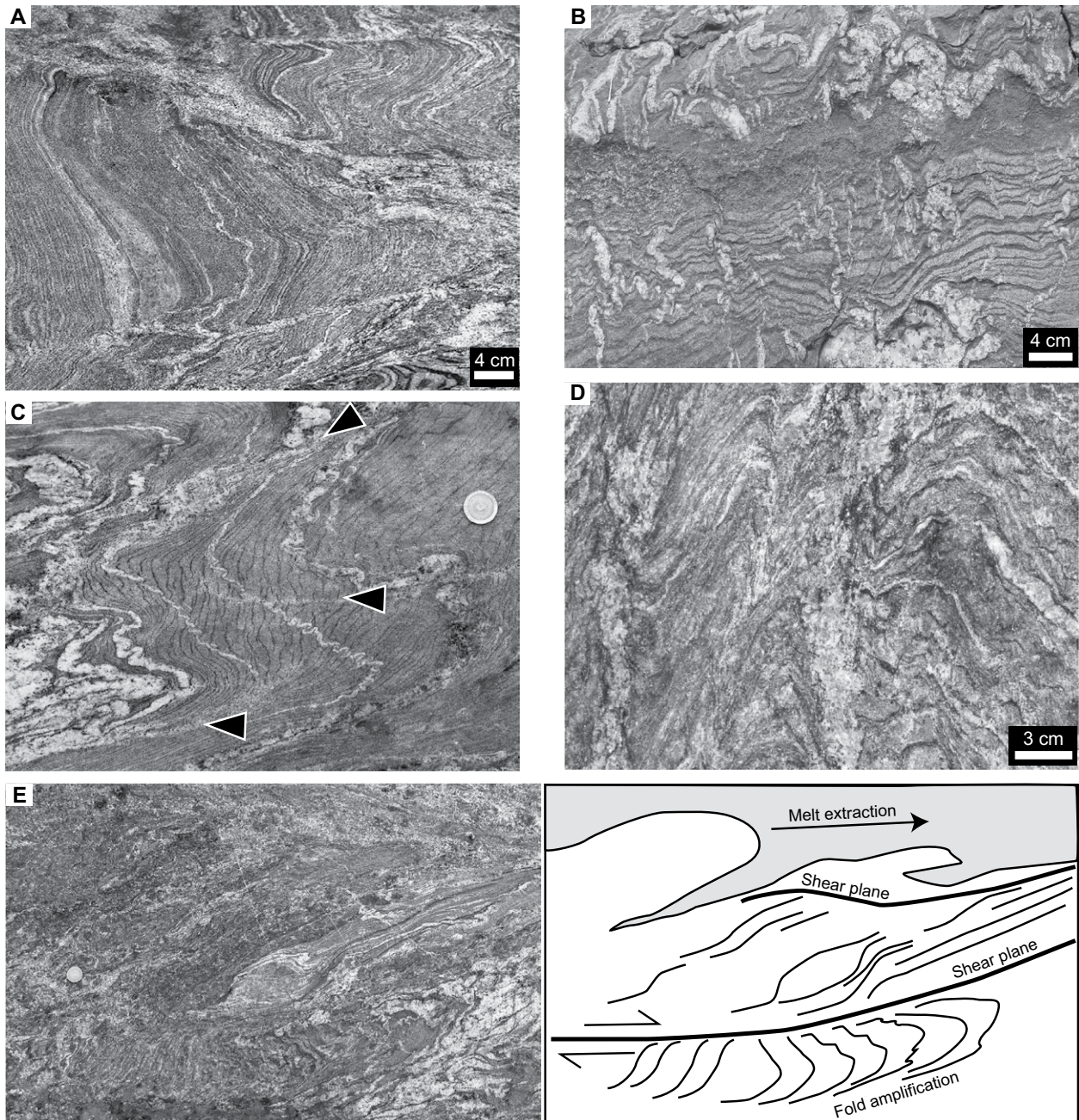


**Figure 7.** Relationship between leucosomes and folds and shearing indicative of synkinematic anatexis. (A) Layered and folded psammite with layer-parallel, thin leucosomes, linked to and bounded by leucosomes parallel to the axial planar orientation of the folds. (B) Layered pelite-psammite sequence with leucosomes cutting across layering, preferentially oriented parallel to axial planar foliation. (C) Folded psammite with early-formed crosscutting leucosomes that define ptygmatic folds. A younger set of leucosomes developed at high angle to these (arrows) and subparallel to axial planar foliation. These have diffuse boundaries with the surroundings and truncate layering and the early-formed, folded leucosomes. (D) Leucosomes in fold limbs linked with thicker leucosomes on axial planes of folds. Views in A to D are approximately perpendicular to the axial plane, and features are interpreted to represent folding and disaggregation of the metasedimentary sequence during melting. (E) Residual metatexite in contact with diatexite and interpretative sketch on the right. Photograph is naturally divided into three horizontal sections: The lower third has a fold that increases in amplitude from left to right, together with an increase in leucosome volume that is concentrated where the fold is tallest on the right, suggesting a response of melt migration to fold growth. The middle third comprises residual, cordierite + garnet-rich pelitic layers, interlayered with psammite, showing asymmetric undulations indicative of top-to-right shearing. The upper band is a heterogeneous cordierite + garnet-diatexite where schlieren define a magmatic flow foliation horizontal across the image. This outcrop shows the many processes of magma migration in response to folding and shearing, leaving behind the complex residual and sheared rocks of the lower part of the photograph, and forming diatexites that flow parallel to the shear plane. View in E is parallel to stretching lineation.

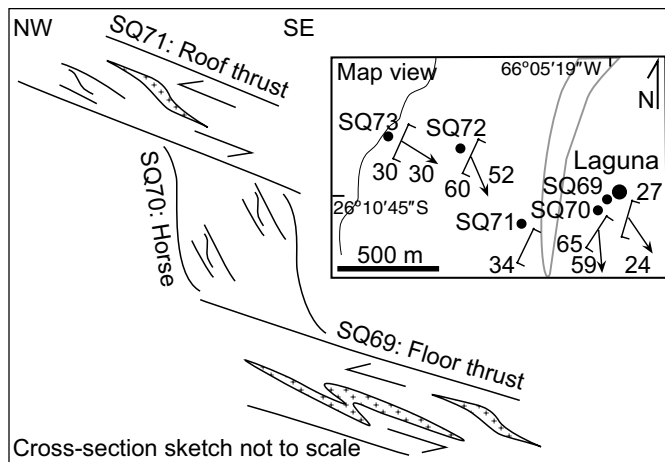


**Figure 8.** Schematic cross section of duplex structure in the orthopyroxene migmatite zone with inset map showing location, also shown in the lower left of Figure 2, in the vicinity of Laguna (see Fig. 2 legend for explanation of symbols).

## Geochronologic Results

Isotopic data are presented in Table 2 and Figures 9 and 10. Twenty-three monazites (25 spots) from SQ37d were analyzed, and they had a range of ages between 501 and 452 Ma, with a mean of  $477 \pm 5$  Ma (mean square of weighted deviates [MSWD] = 9.3 from the line of best fit, probability of fit [ $p$ ] = 0.00; all mean errors reported are  $2\sigma$ , and diagram ellipses are  $1\sigma$ ). Two of the analyses were >10% discordant (Table 2), and their exclusion did not change the mean. Fifteen grains in sample SQ32c were analyzed (17 spots) and revealed a range of ages between 510 and 423 Ma, with a weighted mean of  $478 \pm 12$  Ma (Figs. 9 and 10). Ten of the analyses were >10% discordant (Table 2). Without these points, the range was reduced to 510–460 Ma, with a weighted mean of  $483 \pm 15$  Ma (MSWD = 24,  $p = 0.00$ ). Thirteen monazites (14 spots) were analyzed from SQ84a, and they showed a spread of ages between 492 and 451 Ma, with a weighted mean age of  $475 \pm 7$  Ma (Figs. 9 and 10). Three analyses were >10% discordant (Table 2), and without these, the range was the same, but the mean age was slightly lower,  $472 \pm 7$  Ma (MSWD = 15,  $p = 0.00$ ). Twelve monazites (15 spots) were analyzed from sample SQ181a, the Agua del Sapo schist, and they showed a range of ages between 441 and 410 Ma, with a mean age of  $428 \pm 5$  Ma (Figs. 9 and 10; MSWD = 11.2,  $p = 0.00$ ). None of the analyses were >10% discordant (Table 2).

The high MSWD values indicate that scatter in the data is high, and the low  $p$  values indicate a low probability that the mean age explains the variation in the data, suggesting that it is not representative of the range of age determinations and their errors. This may be a result of multiple age populations within the data set, which can be distinguished using the mixture modeling approach of Sambridge and Compston (1994). This was tested for each data set using the Unmix function of Isoplot (Ludwig, 2008). Two age components were determined for each sample, excluding any results >10% discordant. Each component explained at least 40% of the age population, and the two components were not within error of each other (Fig. 11), indicating the data reflect two age populations. In order to check for additional age populations, models with further components were calculated but found to be redundant, resulting in at least two almost identical ages. The three samples from the El Pichao shear zone showed similar age groups, with an older group with mean ages between 497 and 482 Ma and a younger group between 472 and 461 Ma (Fig. 11). Sample SQ181a also showed two peaks, but the ages were younger, at ca. 435 and 421 Ma (Fig. 11D).

Shear planes are reasonably consistent in orientation, dipping approximately east, with stretching lineations plunging SE or E, gently to steeply (Fig. 2). Occasional west-dipping shear planes, such as those found in lithons in the Opx-migmatite zone, may represent back thrusts or may be related to an earlier shearing event rotated during thrusting. The alternation of steeply and shallowly dipping thrust planes in the Opx-migmatite zone is interpreted as a thrust duplex comprising steeper, less-deformed “horses,” which bend into the shallower roof and floor thrusts, forming an S-shaped geometry in cross section (Fig. 8).

In summary, folds and thrust planes developed contemporaneously with melting in the Tolombón complex and have vergence indicative of top-to-the-west and top-to-the-northwest movement, parallel to the well-defined stretching lineation. As the system cooled, west-directed thrusting localized to the El Pichao shear zone, which thrust these hot rocks over cooler ones (Fig. 3).

## GEOCHRONOLOGY AND MONAZITE GEOCHEMISTRY

Büttner et al. (2005) provided U-Pb, Sm-Nd, Rb-Sr, K-Ar, and  $^{40}\text{Ar}$ - $^{39}\text{Ar}$  age data for rocks between Cafayate and Colalao del Valle (Fig. 1). To complement this data set, we dated rocks close to and within the El Pichao shear zone. Two samples were from intensely sheared rocks from the Tolombón complex: a mylonite (SQ37d:  $26^{\circ}18'59.3''\text{S}$ ,  $66^{\circ}01'07.1''\text{W}$ ) and an ultramylonite (SQ32c:  $26^{\circ}18'37.2''\text{S}$ ,  $66^{\circ}04'05.7''\text{W}$ ). The third sample was an intensely sheared Grt-

schist (SQ84a:  $26^{\circ}20'20.3''\text{S}$ ,  $66^{\circ}02'18.3''\text{W}$ ) at the base of the El Pichao shear zone from the top of the Agua del Sapo complex, intruded by pegmatite dikes that were mylonitized, but lacked evidence for anatexis. We also dated a fourth sample from the footwall of the El Pichao shear zone in the Agua del Sapo complex, an amphibolite facies Bt-Ms-Grt schist (SQ181a:  $26^{\circ}23'37.2''\text{S}$ ,  $66^{\circ}01'27.4''\text{W}$ ). This sample was located 1 km below (perpendicular to strike) the base of the El Pichao shear zone. After dating, monazites were analyzed for trace elements to determine relationships between their composition and ages.

Sample SQ37d is a mylonitic stromatic migmatite that contains leucosomes of Qtz + Kfs + Pl + Grt + Crd and melanosomes of Bt + Qtz + Kfs + Pl + Sil + Ky + Chl with accessory Mnz + Ap + Ilm + Mag. Garnet forms porphyroblasts up to 5 mm in diameter, and the edges of some porphyroblasts are partially replaced by Bt + Chl. A small proportion of biotite (<5%) is partially replaced by chlorite. Sample SQ32c is an ultramylonitic rock formed after granitic diatexite (Finch et al., 2015a) that contains porphyroclasts of Kfs + Pl + Tur in a matrix of Bt + Kfs + Pl + Ms, with accessory Mnz + Ap. Biotite is partially retrogressed to chlorite. Sample SQ84a is a Grt-schist of the Agua del Sapo complex that contains Bt + Qtz + Kfs + Pl + Grt. Garnet porphyroblasts are up to 1 cm in diameter, and biotite and garnet are not retrogressed. Sample SQ181a is a schist from the Agua del Sapo complex and contains Bt + Qtz + Kfs + Pl + Ms + Grt + Tur + Mnz. Garnet porphyroblasts are up to 5 mm in diameter and are partially replaced at their edges by Bt + Chl. Biotite is partially replaced by chlorite.

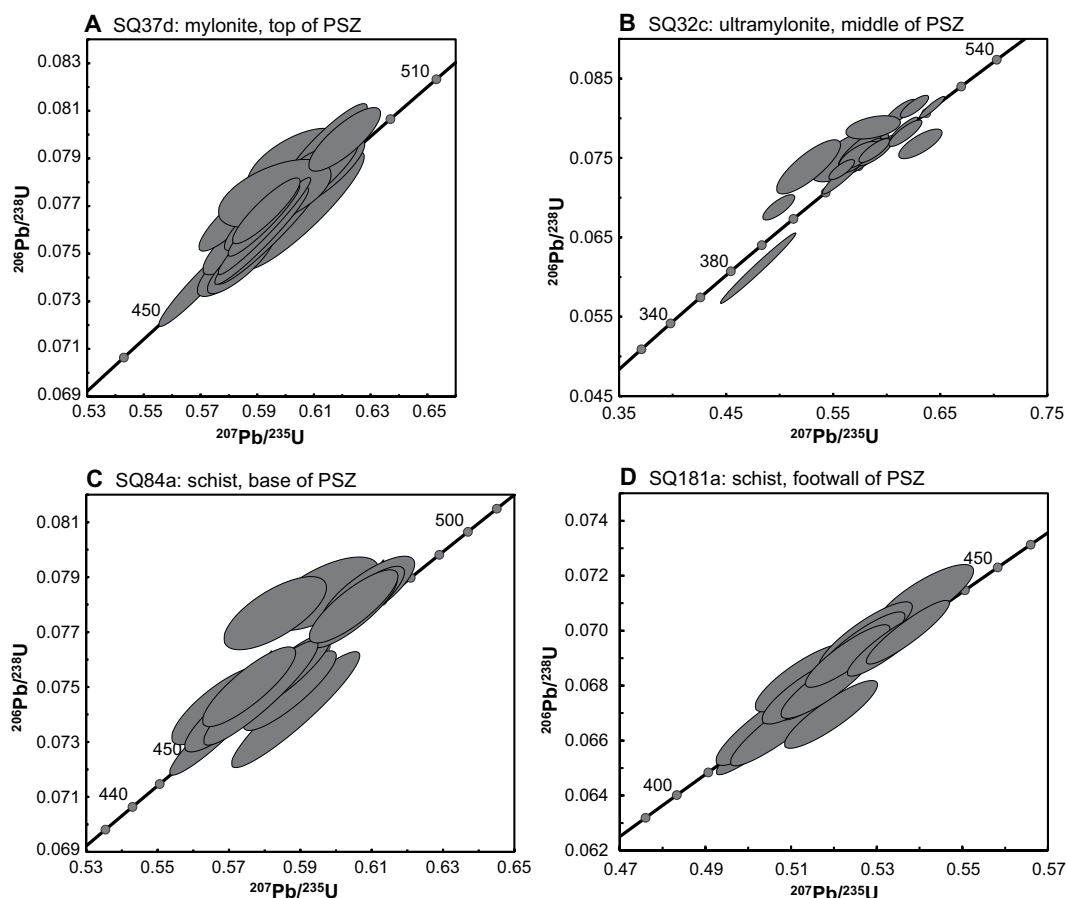


**Figure 9.** Concordia diagrams for the four samples of monazite analyzed from the El Pichao shear zone (PSZ; Table 2). Error ellipses are  $1\sigma$  (68.3% confidence level), and sample locations are indicated in Figures 1 and 3.

In order to determine whether the two age groups in each sample were related to monazite grains that grew at different pressure-temperature conditions, perhaps on the prograde or retrograde path (Rubatto et al., 2013; Kohn, 2014), we analyzed their trace-element composition. The rare earth element (REE) data show wide variation in heavy (H) REEs and a negative Eu anomaly (Fig. 12; GSA Data Repository item DR1<sup>1</sup>), with no systematic geochemical difference between the two age components for any of the samples (Fig. 12).

## DISCUSSION

The origin of high-temperature–low-pressure rocks in back-arcs is the subject of much research and debate, particularly in back-arcs dominated by crustal shortening (e.g., Thompson, 1989; Loosveld and Etheridge, 1990; Collins, 2002; Schulmann et al., 2002; Hyndman et al., 2005; Forbes et al., 2008; Franke, 2014). Questions range from the source of heat in com-

pressive environments (e.g., Lister and Forster, 2009), to the role of tectonic switching between periods of extension and shortening (e.g., Collins, 2002), and the ability of hot back-arcs to sustain mountain belts (Franke, 2014). In this regard, the controversial evolution of the back-arc of the Famatinian orogen could be enlightening. This back-arc is characterized by rocks that reached granulite facies temperatures at pressure not exceeding 6 kbar (e.g., Büttner et al., 2005; Sola et al., 2013). Establishing the relationship between its structural and metamorphic evolution is fundamental to understanding the dynamics of the Famatinian orogeny in particular, and of back-arcs in general.

### Syn-Anatectic Crustal Shortening and Post-Anatectic Strain Localization

The presence of leucosomes parallel to the axial planar orientation of upright and inclined folds and within thrust planes (Fig. 7) suggests that anatexis was contemporaneous with deformation, and that magma migration was controlled by ongoing deformation. Magmas flowed preferentially into those planes and assisted strain accommodation by decreasing

overall flow resistance, and facilitating mass transfer (Weinberg and Mark, 2008). Weinberg et al. (2015) demonstrated that melt accumulation in axial planar orientations, perpendicular to  $\sigma_1$ , can be a result of the compaction of a nonlinear solid rheology with melt-filled pores. When migmatites are shortened, and the rate of fluid flow is lower than the rate of compaction, bands of increased porosity develop that evolve into leucosomes and alternate with compacted bands of decreased porosity (melanosome and mesosome). In addition to these features, there are examples of a coincident increase in fold amplitude with leucosome volume (Fig. 7E), indicating interaction between melt migration and folding. Figure 7 also shows that some of the earlier leucosomes were folded, which we interpret as indicative of an evolving folding event during melting, although more complex alternatives for their origin are possible (e.g., multiple folding events).

The Tolombón thrust and the El Pichao shear zone (Figs. 1 and 2) were post-anatectic and active at amphibolite facies conditions, as indicated by their mineral paragenesis and quartz recrystallization microstructures (Finch et al., 2015a). They record the same kinematics as

<sup>1</sup>GSA Data Repository item 2017188, supplementary table, is available at <http://www.geosociety.org/datarepository/2017> or by request to [editing@geosociety.org](mailto:editing@geosociety.org).

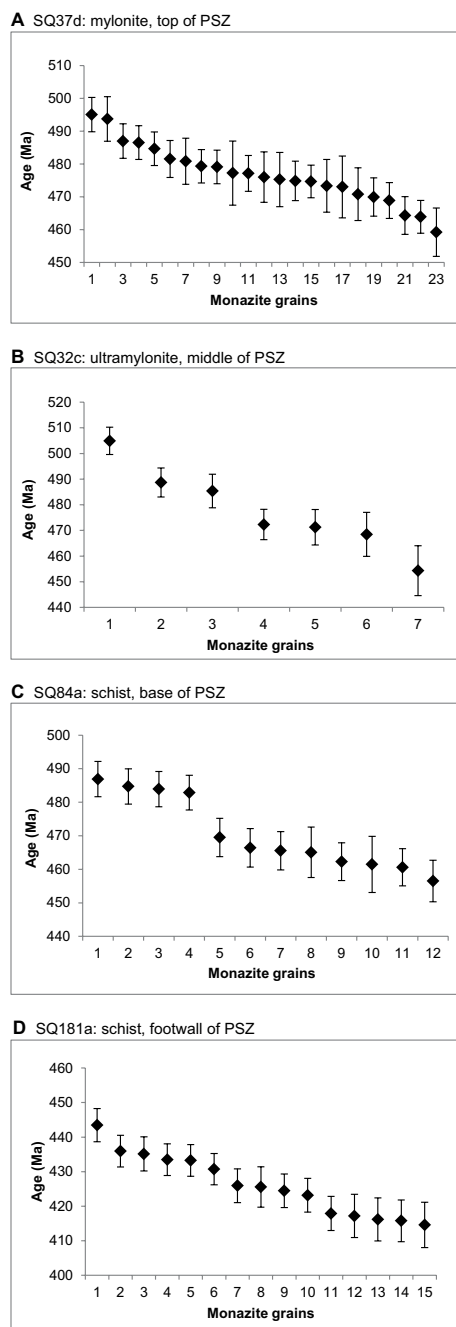


**Figure 10.** U-Pb monazite age of each spot (concordant samples only) with  $1\sigma$  error bars for samples from the El Pichao shear zone (PSZ).

those preserved in the high-grade migmatites (stereonet in Fig. 3). We infer therefore that these shear zones represent a period of localization of the early, syn-anatexis thrusting event, possibly as a result of exhumation and cooling of the package in response to thrusting.

Contrary to this interpretation, Büttner (2009) suggested that shearing was a result of crustal

extension and that the current thrust sense was a result of tilting of subhorizontal planes. He inferred an extensional regime on the basis of telescoped isograds, indicative of crustal thinning. However, telescoping can result from thrusting with a component of shortening perpendicular to the isograds. This process has been reported in the Famatinian Agua Rosada shear zone (50 km NW of Sierra de Quilmes), which also places hotter rocks on cooler rocks (Wegmann et al., 2008). Furthermore, volume loss due to magma removal, as recorded by the residual rocks in migmatites, must also be included when considering the spacing between isograds (Figs. 6B–6F). Thus, our results suggest that peak metamorphism and anatexis occurred during folding, thrusting, and magma extraction related to crustal thickening, and that cooling led to strain localization into amphibolite facies shear zones, which thrust the high-grade Tolombón complex over the lower grade Agua del Sapo complex.

### Geochronology and Peak Metamorphism

Büttner et al. (2005) dated the metamorphic peak in the Tolombón complex migmatites, using U/Pb in monazite (TIMS), and found a single broad age range between ca. 485 and 455 Ma (Fig. 13). Three of their analyses were performed on single large grains, while the others consisted of three or four grains dissolved together. In contrast, U/Pb monazite SHRIMP spot analyses carried out here distinguished two monazite age populations.

Each of the three samples from the El Pichao shear zone show an older and a younger age group. The older group has two almost identical values of  $484.8 \pm 2.3$  Ma and  $484.6 \pm 2.6$  Ma (samples SQ37d and SQ84a) and a third value  $\sim 10$  m.y. older, constrained by only three spot analyses (sample SQ32c). These ages coincide with the onset of bimodal magmatism in the Famatinian magmatic arc in the northern Sierras Pampeanas and the Puna at ca. 485–480 Ma (Hongn and Riller, 2007; Hauser et al., 2011; Hongn et al., 2014), suggesting that this group records increased regional heat flux.

The younger group of ages may simply be a result of partial resetting during a prolonged hot orogeny. Alternatively, the two groups may be meaningful and represent two periods of monazite growth due to (1) two thermal peaks or (2) monazite growth in the prograde path before anatexis (Kohn, 2014), followed by growth during crystallization of the magma in the retrograde path. The lack of clear systematic differences in HREEs or Y between age groups (Fig. 12) suggests that there was no significant change in the partitioning of these elements be-

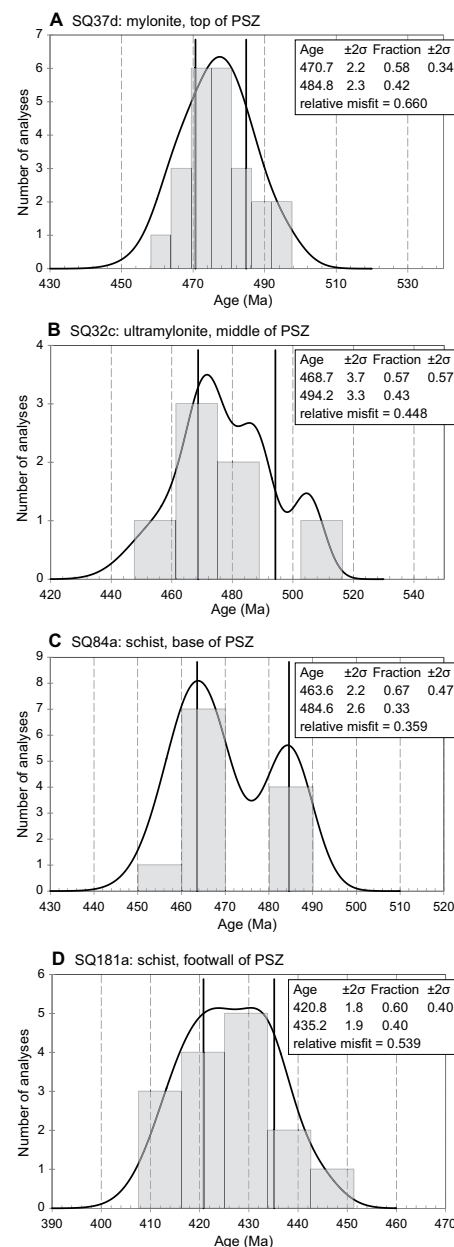


**Figure 11.** U-Pb monazite age probability density plots of the four samples from the El Pichao shear zone (PSZ) analyzed in this study. The ages were calculated using the mixture modeling approach of Sambridge and Compston (1994), where the two vertical lines in each plot represent the mean ages, and the curve is the best fit to the data.

tween garnet and monazite. We therefore suggest that the two age groups either mark two thermal peaks within a long period of metamorphism, or else they may be a result of partial resetting during a prolonged period of orogenesis.

The younger age group of the three El Pichao shear zone samples shows a systematic increase

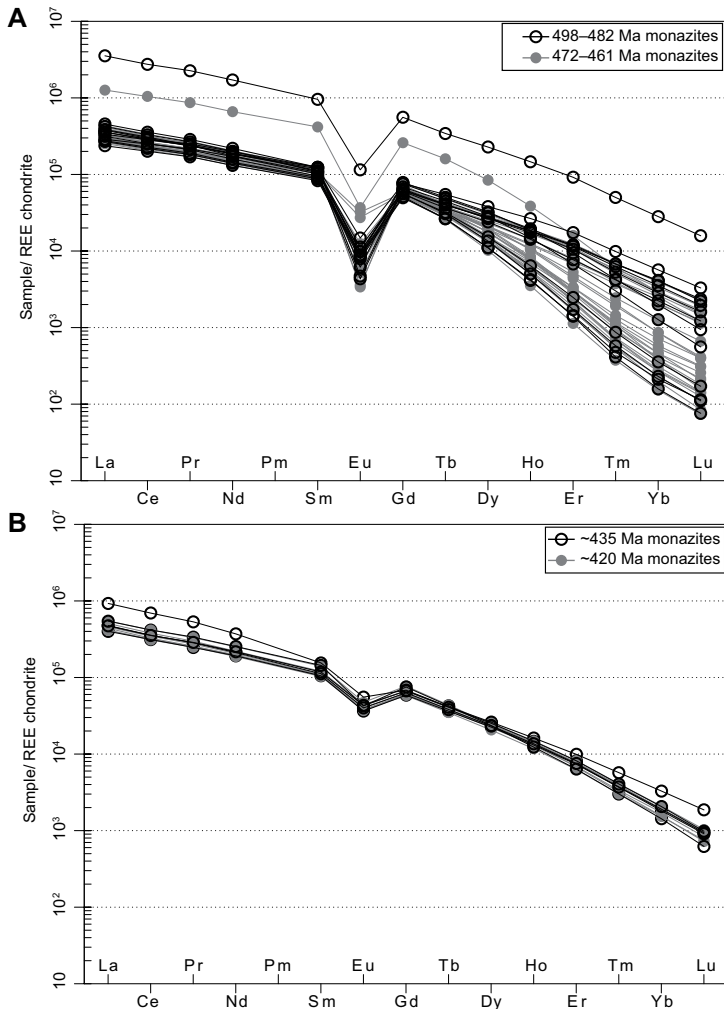
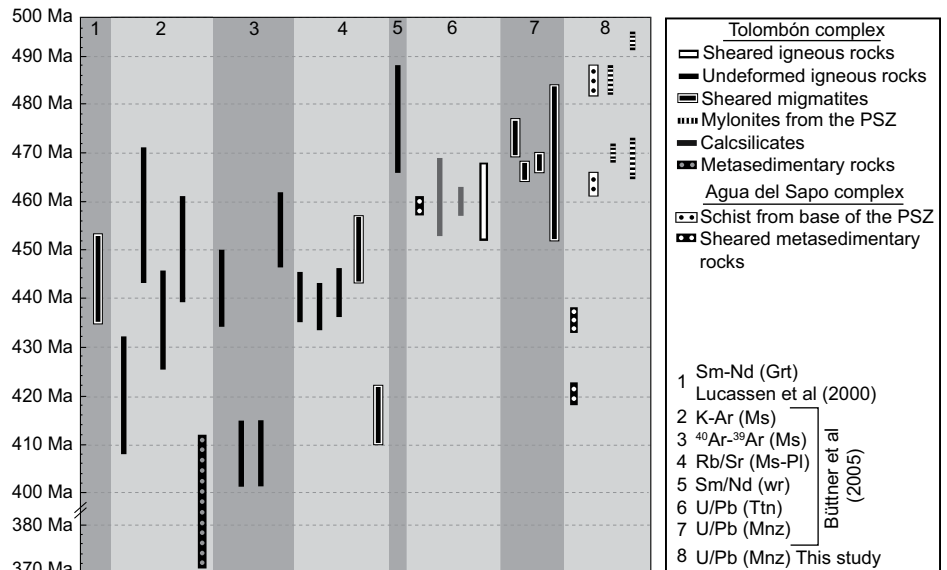


**Figure 12. Chondrite-normalized (Boynnton, 1984) rare earth element (REE) spidergrams for monazite from (A) the three samples from the El Pichao shear zone (PSZ), and (B) the footwall sample. Note that there is no systematic relation between REE pattern and age groups.**

in mean age toward the hanging wall, from  $463.6 \pm 2.2$  Ma (SQ84a) at the base of the shear zone, to  $468.7 \pm 3.7$  Ma (SQ32c) in the middle, and  $470.7 \pm 2.2$  Ma (SQ37d) at the top. It is possible that these ages represent the same central age, and their difference relates to an underestimation of real uncertainties, or that individual spots reflect mixed ages between older and younger sections of the monazite grain. The lack of zonation in BSE images, and the similarity in compositional range, independent of spot age, do not allow elimination of this possibility. Despite this limitation and accepting that the three younger age groups are different, there are a number of possible geological explanations for this trend.

Thrusting on the El Pichao shear zone may have led to rocks cooling from the top down, so that monazite crystallized earlier at the top, as documented in other major thrusts (e.g., the Main Central Thrust in the Himalayas; Kohn, 2014, and references therein). Alternatively, young ages at the base of the shear zone could indicate it was active longer or activated later than the top due to strain localization. The presence of water and its migration through the El Pichao shear zone may have controlled strain localization (Finch et al., 2016), a process that could also cause monazite resetting. The closure temperature of monazite in the presence of an aqueous fluid is as low as  $450^\circ\text{C}$  (Williams et al., 2011). Thus, the availability of water during shearing at amphibolite facies conditions supports the interpretation that the younging-down ages indicate the progression of shearing toward the footwall. The absence of chemical and textural differences between monazites of different ages does not allow us to explore this hypothesis further, so interpretation of the meaning of the younger age groups remains speculative.

**Figure 13. Summary of geochronology data for Sierra de Quilmes; Grt—garnet; Ms—muscovite; Pl—plagioclase; wr—whole rock; Ttn—titanite; Mnz—monazite.**



The two age groups determined for the Agua del Sapó sample SQ181a are markedly younger, suggesting that the footwall stayed hot for longer than the hanging wall, resetting monazite once again. This suggests either a metamorphic response to the thrusting of the Tolombón complex ~30 m.y. after monazite growth in the hanging wall, or that the Agua del Sapó complex was involved in and recorded renewed tectono-metamorphic activity. Delayed timing of peak metamorphism in the footwall compared to the hanging wall is typical of thrust zones. However, the time gap is usually on the order of 5–10 m.y. (e.g., Crowley and Parrish, 1999; Kohn et al., 2001; Mottram et al., 2014), not ~30 m.y. This suggests that thrusting may have continued beyond the time recorded by the monazites in the shear zone and hanging wall, remaining active between ca. 460 and 435 Ma, consistent with other shear zones in the region. For example, the Agua Rosada shear zone was active during granitoid emplacement, dated to 480–455 Ma (Hongn and Riller, 2007), and continued shearing to greenschist facies at 437–428 Ma (Rb-Sr syntectonic white mica; Wegmann et al., 2008). The Arenosa Creek shear zone (~500 km S of Sierra de Quilmes) also began as a high-temperature shear zone and cooled to upper greenschist facies by ca. 445–435 Ma ( $^{40}\text{Ar}/^{39}\text{Ar}$  hornblende; Castro de Machuca et al., 2012).

### Famatinian Orogen and the Ocoyic Tectonic Phase

Previous work (e.g., Bahlburg, 1990; Bahlburg and Hervé, 1997; Coira et al., 2009; Hongn et al., 2014) found that the Famatinian back-arc underwent extension and then shortening, with the switch occurring at ca. 450 Ma. This timing is not borne out by our findings of thrusting contemporaneous with anatexis between 497 and 461 Ma. One-hundred kilometers north of Sierra de Quilmes, in the Sierra de Cachi, a migmatite, a granite, and a gabbro boulder were dated to within error of each other, between 480 and 470 Ma (zircon U/Pb SHRIMP; Hongn et al., 2014). Hongn et al. (2014) interpreted that migmatization and emplacement of granites and gabbros occurred during extension. They based this interpretation on telescoped isograds and high-temperature–low-pressure metamorphism, just as Büttner (2009) did for Sierra de Quilmes. They suggested that the gabbro boulders were indicative of bimodal magmatism, further supporting the interpretation of extension in a back-arc basin. As per our previous discussion, neither the nature of metamorphism nor the telescoping of isograds requires an extensional setting. The finding of gabbro boulders in Sierra

de Cachi reflects the findings of norite blocks in Sierra de Quilmes (Rossi de Toselli et al., 1976), and the inference of bimodal magmatism requires further investigation. We note that Hongn et al. (2014) also described thrusting in Sierra de Cachi, indicating a period of shortening post-dating extension and peak metamorphism, placing already cool higher grade rocks structurally above lower grade rocks. A similar switch could have occurred in Sierra de Quilmes (but earlier than in Cachi), but any period of extension left little structural evidence. While we are unable to tightly constrain the onset of thrusting in Sierra de Quilmes, it demonstrably began during or before peak metamorphism (>460 Ma), preceding the start of the Ocoyic tectonic phase at ca. 450 Ma. Adding support to our findings, several other Famatinian thrusts seem to predate the Ocoyic tectonic phase, including the 515–417 Ma shear zones in Sierra de Pie de Palo (SW Sierras Pampeanas; Mulcahy et al., 2011) and the 480–424 Ma Agua Rosada shear zone.

While a period of Early Ordovician extension is well defined in some regions (e.g., Puna and Cordillera Oriental bimodal volcanism and thick sedimentary sequences; Bahlburg, 1990, 1991; Coira et al., 2009), in others, evidence for extension is unclear, and the “Ocoyic tectonic phase” cannot be differentiated from the rest of the Famatinian orogeny. This may be a result of the preservation of shallower crustal levels in the Puna and the Cordillera Oriental, while the southern Sierras Pampeanas preserves only deeper sections, where pervasive ductile deformation during shortening may have obliterated earlier structures. Alternatively, it is possible that some areas of the Famatinian back-arc were undergoing shortening while others were extending, suggesting a complex spatial and temporal distribution of deformation.

### Heat in the Sierra de Quilmes

High-temperature–low-pressure metamorphism in convergent mobile belts may be a result of (1) an earlier period of lithospheric thinning including convective thinning (e.g., Loosveld and Etheridge, 1990), (2) contact metamorphism with arc magmas (e.g., Alasino et al., 2014), or (3) devolatilization of the downgoing slab, causing increased rates of shallow asthenospheric convection (Hyndman et al., 2005). We find that all three are possible, but evidence for extension and arc-related intrusive rocks, at least in Sierra de Quilmes, is lacking, although hot intrusions could have underplated the extensive migmatite with little evidence (see Riel et al., 2016).

Ancient back-arcs are purported to be a prerequisite for the development of an orogenic root, because their hot, thin lithospheres allow

strong strain localization (Schulmann et al., 2002). However, through most of the Famatinian Orogen, the exposed crustal level lacks high-pressure rocks, suggesting either that the deepest crustal levels are not exposed, or that pronounced crustal thickening did not occur. Crustal thickening may be prevented where there is intensive partial melting, which weakens the crust and prevents significant stacking (Franke, 2014). Most likely, there is a spectrum of back-arc heat flux conditions: At one end of the continuum, heat flux is moderate, and the crust can be stacked, leading to mountain building, whereas at the other extreme, high heat flux renders the crust too weak, resulting in “failed orogens” (Franke, 2014). We suggest Sierra de Quilmes lies between these two extremes: Rocks were competent enough to allow thrusting and modest stacking, but they were too weak to form a thick orogenic root.

### CONCLUSION

The geology of the Sierra de Quilmes suggests that deformation started during peak metamorphism contemporaneous with granulite facies anatexis. Deformation was characterized by top-to-the-W or -NW thrusting and verging folds, and continued as the rocks cooled to amphibolite facies and shearing localized to major thrust zones. Synkinematic anatexis led to magma migration through networks in which magma fractionated during migration, accumulating to form diatexites and granites and leaving behind highly residual rocks.

Two periods of monazite crystallization are recorded in the mylonitic rocks of the El Pichao shear zone at 497–482 Ma and 472–461 Ma. These groups may be the result of partial resetting during a prolonged, hot orogenesis. Alternatively, they may represent two distinct periods of monazite growth, suggesting either two thermal peaks or monazite rejuvenation during shearing within the El Pichao shear zone. The considerably younger ages of monazite in the Agua del Sapó complex (435–420 Ma) suggest monazite resetting or growth in the footwall in response to either thrusting of the Tolombón complex or a renewed tectono-thermal event. This possible late movement on the El Pichao shear zone could have coincided with the activation of other shear zones in the region, suggesting a widespread shortening event throughout the Sierras Pampeanas, perhaps coincident with collision of the Cuyania terrane in the southern Sierras Pampeanas. The high heat flux responsible for the high-temperature–low-pressure metamorphism substantially weakened the crust, impeding significant crustal thickening, and resulting in wide exposures of cordierite-bearing migma-

tites. We suggest that Sierra de Quilmes was part of a compressional back-arc section during most of the Famatinian orogeny, contrary to other regions within the back-arc, where extension was dominant. It seems likely that the evolution of the Famatinian back-arc was characterized by a nonuniform spatial distribution of extension and shortening varying through time.

#### ACKNOWLEDGMENTS

We thank Mariano A. Larrovere and an anonymous reviewer for careful and helpful reviews. Juan E. Otamendi and Steffen H. Büttner are thanked for reviews of an earlier version, Massimo Reveggi for assistance with the collection of the laser ablation–inductively coupled plasma–mass spectrometry data, and Colin MacRae for assistance with collection of the microprobe data. Hasalová acknowledges funding from the Czech Science Foundation (GACR grant 14-25995S).

#### REFERENCES CITED

- Aceñolaza, F.G., and Toselli, A., 1973, Stratigraphic and tectonic considerations concerning the Lower Paleozoic of northwestern Argentina: *II Congreso Latinoamericano de Geología, Memorias*, v. 2, p. 755–763.
- Alasino, P.H., Casquet, C., Larrovere, M.A., Pankhurst, R., Galindo, C., Dahlquist, J., Baldo, E., and Rapela, C.W., 2014, The evolution of a mid-crustal thermal aureole at Cerro Toro, Sierra de Famatina, NW Argentina: *Lithos*, v. 190–191, p. 154–172, doi:10.1016/j.lithos.2013.12.006.
- Astini, R.A., and Dávila, F.M., 2004, Ordovician back arc foreland and Ocoyoc thrust belt development on the western Gondwana margin as a response to Precordillera terrane accretion: *Tectonics*, v. 23, TC4008, doi:10.1029/2003TC001620.
- Bahlburg, H., 1990, The Ordovician basin in the Puna of NW Argentina and N Chile: Geodynamic evolution from back-arc to foreland basin: *Geotektonische Forschungen*, v. 75, p. 1–107.
- Bahlburg, H., 1991, The Ordovician back-arc to foreland successor basin in the Argentinian-Chilean Puna: Tectono-sedimentary trends and sea-level changes, in Macdonald, D.I.M., ed., *Sedimentation, Tectonics and Eustasy: Sea-Level Changes at Active Margins*: International Association of Sedimentologists Special Publication 12, p. 465–484.
- Bahlburg, H., and Hervé, F., 1997, Geodynamic evolution and tectonostratigraphic terranes of northwestern Argentina and northern Chile: *Geological Society of America Bulletin*, v. 109, no. 7, p. 869–884, doi:10.1130/0016-7606(1997)109<0869:GEATTO>2.3.CO;2.
- Becchio, R., and Lucassen, F., 2002, Concordant titanite U-Pb ages of Cambrian to Silurian high-T metamorphism at the western edge of Gondwana (Southern Puna and western Sierras Pampeanas, Argentina, 26–29°), in 5th International Symposium on Andean Geodynamics: Toulouse, France.
- Bellos, L.I., Castro, A., Díaz-Alvarado, J., and Toselli, A., 2015, Multi-pulse cotectic evolution and in-situ fractionation of calc-alkaline tonalite-granodiorite rocks, Sierra de Velasco batholith, Famatinian belt, Argentina: *Gondwana Research*, v. 27, no. 1, p. 258–280, doi:10.1016/j.gr.2013.09.019.
- Boynton, W.V., 1984, Cosmochemistry of the rare earth elements: Meteorite studies, in Henderson, P., ed., *Rare Earth Element Geochemistry*: Amsterdam, Netherlands, Elsevier, p. 63–114, doi:10.1016/B978-0-444-42148-7.50008-3.
- Büttner, S.H., 2009, The Ordovician Sierras Pampeanas–Puna basin connection: Basement thinning and basin formation in the proto-Andean back-arc: *Tectonophysics*, v. 477, no. 3–4, p. 278–291, doi:10.1016/j.tecto.2009.02.003.
- Büttner, S.H., 2015, Comment: “One kilometre-thick ultramylonite, Sierra de Quilmes, Sierras Pampeanas, NW Argentina” by M.A. Finch, R.F. Weinberg, M.G. Fuentes, P. Hasalova, and R. Becchio (*Journal of Structural Geology* 72 [2015] 33–54): *Journal of Structural Geology*, v. 76, p. 80–83, doi:10.1016/j.jsg.2015.04.003.
- Büttner, S.H., Glodny, J., Lucassen, F., Wemmer, K., Erdmann, S., Handler, R., and Franz, G., 2005, Ordovician metamorphism and plutonism in the Sierra de Quilmes metamorphic complex: Implications for the tectonic setting of the northern Sierras Pampeanas (NW Argentina): *Lithos*, v. 83, no. 1–2, p. 143–181, doi:10.1016/j.lithos.2005.01.006.
- Castro de Machuca, B., Delpino, S., Previley, L., Mogessie, A., and Bjerg, E., 2012, Tectono-metamorphic evolution of a high- to medium-grade ductile deformed metagabbro/metadiorite from the Arenosa Creek shear zone, western Sierras Pampeanas, Argentina: *Journal of Structural Geology*, v. 42, p. 261–278, doi:10.1016/j.jsg.2012.04.010.
- Coira, B., Kirschbaum, A., Hongn, F., Pérez, B., and Mene-gatti, N., 2009, Basic magmatism in northeastern Puna, Argentina: Chemical composition and tectonic setting in the Ordovician back-arc: *Journal of South American Earth Sciences*, v. 28, no. 4, p. 374–382, doi:10.1016/j.jsames.2009.04.007.
- Collins, W.J., 2002, Hot orogens, tectonic switching, and creation of continental crust: *Geology*, v. 30, p. 535–538, doi:10.1130/0091-7613(2002)030<0535:HOTSAC>2.0.CO;2.
- Crowley, J.L., and Parrish, R.R., 1999, U-Pb isotopic constraints on diachronous metamorphism in the northern Monashee complex, southern Canadian Cordillera: *Journal of Metamorphic Geology*, v. 17, no. 5, p. 483–502, doi:10.1046/j.1525-1314.1999.00210.x.
- Finch, M.A., Weinberg, R.F., Fuentes, M.G., Hasalova, P., and Becchio, R., 2015a, One kilometre-thick ultramylonite, Sierra de Quilmes, Sierras Pampeanas, NW Argentina: *Journal of Structural Geology*, v. 72, p. 33–54, doi:10.1016/j.jsg.2015.01.002.
- Finch, M.A., Weinberg, R.F., Fuentes, M.G., Hasalova, P., and Becchio, R., 2015b, Reply to comment by S.H. Büttner on: “One kilometre-thick ultramylonite, Sierra de Quilmes, Sierras Pampeanas, NW Argentina”: *Journal of Structural Geology*, v. 76, p. 84–85, doi:10.1016/j.jsg.2015.04.004.
- Finch, M.A., Weinberg, R.F., and Hunter, N.J.R., 2016, Water loss and the origin of thick ultramylonites: *Geology*, v. 44, no. 8, p. 599–602, doi:10.1130/G37972.1.
- Forbes, C.J., Betts, P.G., Giles, D., and Weinberg, R.F., 2008, Reinterpretation of the tectonic context of high-temperature metamorphism in the Broken Hill block, NSW, and implication on the Palaeo- to Mesoproterozoic evolution: *Precambrian Research*, v. 166, p. 338–349, doi:10.1016/j.precamres.2006.12.017.
- Franke, W., 2014, Topography of the Variscan orogen in Europe: Failed, not collapsed: *International Journal of Earth Sciences*, v. 103, no. 5, p. 1471–1499.
- Green, T.H., 1976, Experimental generation of cordierite- or garnet-bearing granitic liquids from a pelitic composition: *Geology*, v. 4, no. 2, p. 85–88, doi:10.1130/0091-7613(1976)4<85:EGOCGG>2.0.CO;2.
- Hauser, N., Matteini, M., Omarini, R.H., and Pimentel, M.M., 2011, Combined U-Pb and Lu-Hf isotope data on turbidites of the Paleozoic basement of NW Argentina and petrology of associated igneous rocks: Implications for the tectonic evolution of western Gondwana between 560 and 460 Ma: *Gondwana Research*, v. 19, p. 100–127, doi:10.1016/j.gr.2010.04.002.
- Höckenreiner, M., Söllner, F., and Miller, H., 2003, Dating the TIPA shear zone: An Early Devonian terrane boundary between the Famatinian and Pampean systems (NW Argentina): *Journal of South American Earth Sciences*, v. 16, no. 1, p. 45–66, doi:10.1016/S0895-9811(03)00018-X.
- Hongn, F.D., and Riller, U., 2007, Tectonic evolution of the western margin of Gondwana inferred from syntectonic emplacement of Paleozoic granitoid plutons in northwest Argentina: *The Journal of Geology*, v. 115, no. 2, p. 163–180, doi:10.1086/510644.
- Hongn, F.D., Tubia, J.M., Esteban, J.J., Aranguren, A., Vegas, N., Sergeev, S., Larionov, A., and Basci, M., 2014, The Sierra de Cachi (Salta, NW Argentina): Geological evidence about a Famatinian retro-arc at mid crustal levels: *Journal of Iberian Geology*, v. 40, no. 2, p. 225–240, doi:10.5209/rev\_JIGE.2014.v40.n2.45303.
- Hyndman, R.D., Currie, C.A., and Mazzotti, S.P., 2005, Subduction zone backarcs, mobile belts, and orogenic heat: *GSA Today*, v. 15, no. 2, p. 4–10, doi:10.1130/1052-5173(2005)015<4:SZBMBMA>2.0.CO;2.
- Katz, M.B., 1985, The tectonics of Precambrian craton-mobile belts: Progressive deformation of polygonal miniplates: *Precambrian Research*, v. 27, no. 4, p. 307–319, doi:10.1016/0301-9268(85)90091-9.
- Knüver, M., and Miller, H., 1981, Ages of metamorphic and deformational events in the Sierra de Ancasti (Pampean Ranges; Argentina): *Geologische Rundschau*, v. 70, no. 3, p. 1020–1029, doi:10.1007/BF01820178.
- Kohn, M.J., 2014, Himalayan metamorphism and its tectonic implications: *Annual Review of Earth and Planetary Sciences*, v. 42, p. 381–419, doi:10.1146/annurev-earth-060313-055005.
- Kohn, M.J., Catlos, E.J., Ryerson, F.J., and Harrison, T.M., 2001, Pressure-temperature-time path discontinuity in the Main Central thrust zone, central Nepal: *Geology*, v. 29, no. 7, p. 571–574, doi:10.1130/0091-7613(2001)029<0571:PTTDPDI>2.0.CO;2.
- Korhonen, F.J., Saw, A.K., Clark, C., Brown, M., and Bhattacharya, S., 2011, New constraints on UHT metamorphism in the Eastern Ghats Province through the application of phase equilibria modelling and in situ geochronology: *Gondwana Research*, v. 20, no. 4, p. 764–781, doi:10.1016/j.gr.2011.05.006.
- Kretz, R., 1983, Symbols for rock-forming minerals: *The American Mineralogist*, v. 68, p. 277–279.
- Kriegsman, L.M., 2001, Partial melting, partial melt extraction and partial back reaction in anatectic migmatites: *Lithos*, v. 56, p. 75–96, doi:10.1016/S0024-4937(00)00060-8.
- Larrovere, M.A., de los Hoyos, C.R., Toselli, A.J., Rossi, J.N., Basci, M.A.S., and Belmar, M.E., 2011, High TP evolution and metamorphic ages of the migmatitic basement of northern Sierras Pampeanas, Argentina: Characterization of a mid-crustal segment of the Famatinian belt: *Journal of South American Earth Sciences*, v. 31, no. 2–3, p. 279–297, doi:10.1016/j.jsames.2010.11.006.
- Larrovere, M.A., Alasino, P.H., and Baldo, E.G., 2016, La faja de cizalla dúctil doble-vergente del noroeste de la Sierra de Velasco: Deformación de la corteza media durante la orogenia Famatiniana: *Revista de la Asociación Geológica Argentina*, v. 73, p. 117–133.
- Lister, G., and Forster, M., 2009, Tectonic mode switches and the nature of orogenesis: *Lithos*, v. 113, p. 274–291, doi:10.1016/j.lithos.2008.10.024.
- Loosveld, R.J.H., and Etheridge, M.A., 1990, A model for low-pressure facies metamorphism during crustal thickening: *Journal of Metamorphic Geology*, v. 8, no. 3, p. 257–267, doi:10.1111/j.1525-1314.1990.tb00472.x.
- Lucassen, F., Becchio, R., Wilke, H.G., Franz, G., Thirlwall, M.F., Viramonte, J., and Wemmer, K., 2000, Proterozoic–Paleozoic development of the basement of the Central Andes (18–26°S)—A mobile belt of the South American craton: *Journal of South American Earth Sciences*, v. 13, p. 697–715, doi:10.1016/S0895-9811(00)00057-2.
- Ludwig, K.R., 2008, *Isoplot/Ex Version 4.0: A Geochronological Toolkit for Microsoft Excel*: Berkeley Geochronology Center Special Publication 4.
- Miller, C., Pankhurst, R., Rapela, C., Saavedra, J., and Toselli, A., 1991, Genesis de los granitoides Paleozoicos peraluminosos areas Tafi del Valle y Cafayate, Sierras Pampeanas, Argentina, in *Actas 6th Congreso Geológico Chileno*, v. 1: Santiago, Chile, Servicio Nacional de Geología y Minería, p. 36–39.
- Mottram, C.M., Warren, C.J., Regis, D., Roberts, N.M.W., Harris, N.B.W., Argles, T.W., and Parrish, R.R., 2014, Developing an inverted Barrovian sequence: insights from monazite petrochronology: *Earth and Planetary Science Letters*, v. 403, p. 418–431, doi:10.1016/j.epsl.2014.07.006.
- Moya, M.C., 1988, Lower Ordovician in the southern part of the Argentine Eastern Cordillera, in Bahlburg, H., Breitkreuz, C., and Giese, P., eds., *The Southern Central Andes*: Berlin, Springer, p. 55–69, doi:10.1007/BFb0045174.

- Mulcahy, S.R., Roeske, S.M., McClelland, W.C., Jourdan, F., Iriondo, A., Renne, P.R., Vervoort, J.D., and Vujovich, G.I., 2011, Structural evolution of a composite middle to lower crustal section: The Sierra de Pie de Palo, northwest Argentina: *Tectonics*, v. 30, TC1005, doi:10.1029/2009TC002656.
- Pankhurst, R.J., Rapela, C.W., Saavedra, J., Baldo, E., Dahlquist, J., Pascua, I., and Fanning, C.M., 1998, The Famatinian magmatic arc in the central Sierras Pampeanas: An Early to Mid-Ordovician continental arc on the Gondwana margin, in Pankhurst, R.J., and Rapela, C.W., eds., *The Proto-Andean Margin of Gondwana*: Geological Society, London, Special Publication 142, p. 343–367, doi:10.1144/GSL.SP.1998.142.01.17.
- Pankhurst, R.J., Rapela, C.W., and Fanning, C.M., 2000, Age and origin of coeval TTG, I- and S-type granites in the Famatinian belt of NW Argentina: *Earth and Environmental Science Transactions of the Royal Society of Edinburgh*, v. 91, no. 1-2, p. 151–168, doi:10.1017/S0263593300007343.
- Powell, R., and Holland, J.B., 1990, Calculated mineral equilibria in the pelitic system, KFMASH (K<sub>2</sub>O-FeO-MgO-Al<sub>2</sub>O<sub>3</sub>-SiO<sub>2</sub>-H<sub>2</sub>O): *The American Mineralogist*, v. 75, p. 367–380.
- Rapela, C., 1976, El basamento metamórfico de la región de Cafayate, Provincia de Salta. Aspectos petrológicos y geoquímicos: *Revista de la Asociación Geológica Argentina*, v. 31, p. 203–222.
- Rapela, C.W., and Shaw, D.M., 1979, Trace and major element models of granitoid genesis in the Pampean Ranges, Argentina: *Geochimica et Cosmochimica Acta*, v. 43, no. 7, p. 1117–1129, doi:10.1016/0016-7037(79)90098-X.
- Rapela, C.W., Heaman, L.M., and McNutt, R.H., 1982, Rb-Sr geochronology of granitoid rocks from the Pampean Ranges, Argentina: *The Journal of Geology*, v. 90, no. 5, p. 574–582, doi:10.1086/628714.
- Rapela, C.W., Pankhurst, R.J., Casquet, C., Baldo, E., Saavedra, J., and Galindo, C., 1998a, Early evolution of the proto-Andean margin of South America: *Geology*, v. 26, no. 8, p. 707–710, doi:10.1130/0091-7613(1998)026<0707:EEOTPA>2.3.CO;2.
- Rapela, C.W., Pankhurst, R.J., Casquet, C., Baldo, E., Saavedra, J., Galindo, C., and Fanning, C.M., 1998b, The Pampean orogeny of the southern proto-Andes: Cambrian continental collision in the Sierras de Cordoba, in Pankhurst, R.J., and Rapela, C.W., eds., *The Proto-Andean Margin of Gondwana*: Geological Society of London, Special Publication 142, p. 181–217, doi:10.1144/GSL.SP.1998.142.01.10.
- Rapela, C.W., Verdecchia, S.O., Casquet, C., Pankhurst, R.J., Baldo, E.G., Galindo, C., Murra, J.A., Dahlquist, J.A., and Fanning, C.M., 2016, Identifying Laurentian and SW Gondwana sources in the Neoproterozoic to early Paleozoic metasedimentary rocks of the Sierras Pampeanas: Paleogeographic and tectonic implications: *Gondwana Research*, v. 32, p. 193–212, doi:10.1016/j.gr.2015.02.010.
- Riel, N., Mercier, J., and Weinberg, R.F., 2016, Convection in a partially molten metasedimentary crust? Insights from the El Oro complex (Ecuador): *Geology*, v. 44, p. 31–34, doi:10.1130/G37208.1.
- Rossi de Toselli, J.N., Toselli, A., and Toselli, G., 1976, Migmatización y metamorfismo en el basamento de la Sierra de Quilmes, al oeste de Colalao del Valle, Provincia de Tucumán, Argentina: *Revista de la Asociación Geológica Argentina*, v. 31, no. 2, p. 83–94.
- Rubatto, D., Chakraborty, S., and Dasgupta, S., 2013, Timescales of crustal melting in the Higher Himalayan Crystallines (Sikkim, Eastern Himalaya) inferred from trace element–constrained monazite and zircon chronology: *Contributions to Mineralogy and Petrology*, v. 165, p. 349–372, doi:10.1007/s00410-012-0812-y.
- Sambridge, M.S., and Compston, W., 1994, Mixture modeling of multi-component data sets with application to ion-probe zircon ages: *Earth and Planetary Science Letters*, v. 128, p. 373–390, doi:10.1016/0012-821X(94)90157-0.
- Sawyer, E.W., 1998, Formation and evolution of granite magmas during crustal reworking: The significant of diatexites: *Journal of Petrology*, v. 39, no. 6, p. 1147–1167, doi:10.1093/ptroj/39.6.1147.
- Sawyer, E.W., 2008, Atlas of Migmatites: Canadian Mineralogist Special Publication 9, 371 p.
- Schulmann, K., Schaltegger, U., Jezek, J., Thompson, A.B., and Edel, J.-B., 2002, Rapid burial and exhumation during orogeny: Thickening and synconvergent exhumation of thermally weakened and thinned crust (Variscan orogen in Western Europe): *American Journal of Science*, v. 302, no. 10, p. 856–879, doi:10.2475/ajs.302.10.856.
- Simpson, C., Law, R.D., Gromet, L.P., Miro, R., and Northrup, C.J., 2003, Paleozoic deformation in the Sierras de Cordoba and Sierra de Las Minas, eastern Sierras Pampeanas, Argentina: *Journal of South American Earth Sciences*, v. 15, no. 7, p. 749–764, doi:10.1016/S0895-9811(02)00130-X.
- Sola, A.M., Becchio, R.A., and Pimentel, M., 2013, Petrogenesis of migmatites and leucogranites from Sierra de Molinos, Salta, northwest Argentina: A petrologic and geochemical study: *Lithos*, v. 177, no. 1, p. 470–491, doi:10.1016/j.lithos.2013.07.025.
- Stern, R.A., and Berman, R.G., 2001, Monazite U-Pb and Th-Pb geochronology by ion microprobe, with an application to in situ dating of an Archean metasedimentary rock: *Chemical Geology*, v. 172, no. 1-2, p. 113–130, doi:10.1016/S0009-2541(00)00239-4.
- Thomas, W.A., and Astini, R.A., 1996, The Argentine Precordillera: A traveler from the Ouachita embayment of North America: *Laurentia: Science*, v. 273, p. 752–757.
- Thomas, W.A., and Astini, R.A., 2003, Ordovician accretion of the Argentine Precordillera terrane to Gondwana: A review: *Journal of South American Earth Sciences*, v. 16, no. 1, p. 67–79, doi:10.1016/S0895-9811(03)00019-1.
- Thompson, P.H., 1989, Moderate overthickening of thinned sialic crust and the origin of granitic magmatism and regional metamorphism in low-*P*–high-*T* terranes: *Geology*, v. 17, no. 6, p. 520–523, doi:10.1130/0091-7613(1989)017<0520:MOOTSC>2.3.CO;2.
- Toselli, A., Rossi De Toselli, J.N., and Rapela, C.W., 1978, El basamento metamórfico de la Sierra de Quilmes, Republica Argentina: *Revista de la Asociación Geológica Argentina*, v. 33, no. 2, p. 105–121.
- Turner, J.C., 1960, Estratigrafía de la Sierra de Santa Victoria y adyacencias: *Boletín de la Academia Nacional de Ciencias, Córdoba*, v. 41, no. 2, p. 163–206.
- Turner, J.C.M., and Méndez, V., 1975, Geología del sector oriental de los Departamentos de Santa Victoria e Iruya, Provincia de Salta: Republica Argentina: *Boletín Academia Nacional de Ciencias de Córdoba*, v. 51, p. 11–24.
- Van Achtenbergh, E., Ryan, C.G., Jackson, S.E., and Griffin, W.L., 2001, Data reduction software for LA-ICP-MS: Appendix, in Sylvester, P.J., ed., *Laser Ablation-ICP-Mass Spectrometry in the Earth Sciences: Principles and Applications*: Ottawa, Ontario, Canada, Mineralogical Association of Canada Short Course 29, p. 239–243.
- Varela, R., Basei, M.S., González, P., Sato, A., Naipauer, M., Campos Neto, M., Cingolani, C., and Meira, V., 2011, Accretion of Grenvillian terranes to the southwestern border of the Río de la Plata craton, western Argentina: *International Journal of Earth Sciences*, v. 100, no. 2-3, p. 243–272, doi:10.1007/s00531-010-0614-2.
- Vernon, R.H., 2004, *A Practical Guide to Rock Microstructure*: New York, Cambridge University Press, 606 p., doi:10.1017/CBO9780511807206.
- Vielzeuf, D., and Holloway, J.R., 1988, Experimental determination of the fluid-absent melting relations in the pelitic system: *Contributions to Mineralogy and Petrology*, v. 98, no. 3, p. 257–276, doi:10.1007/BF00375178.
- Vielzeuf, D., and Montel, J.M., 1994, Experimental constraints on partial melting in the crust: *Mineralogical Magazine*, v. 58A, p. 940–941, doi:10.1180/minmag.1994.58A.2.224.
- Wegmann, M.I., Riller, U., Hongn, F.D., Glodny, J., and Oncken, O., 2008, Age and kinematics of ductile deformation in the Cerro Durazno area, NW Argentina: Significance for orogenic processes operating at the western margin of Gondwana during Ordovician–Silurian times: *Journal of South American Earth Sciences*, v. 26, no. 1, p. 78–90, doi:10.1016/j.jsames.2007.12.004.
- Weinberg, R.F., and Mark, G., 2008, Magma migration, folding and disaggregation of migmatites in the Karakoram shear zone, Ladakh, NW India: *Geological Society of America Bulletin*, v. 120, p. 994–1009, doi:10.1130/B26227.1.
- Weinberg, R.F., Veveakis, E., and Regenauer-Lieb, K., 2015, Compaction-driven melt segregation in migmatites: *Geology*, v. 43, no. 6, p. 471–474, doi:10.1130/G36562.1.
- White, R.W., and Powell, R., 2010, Retrograde melt-residue interaction and the formation of near-anhydrous leucosomes in migmatites: *Journal of Metamorphic Geology*, v. 28, p. 579–597, doi:10.1111/j.1525-1314.2010.00881.x.
- Wickham, S.M., and Oxburgh, E.R., 1985, Continental rifts as a setting for regional metamorphism: *Nature*, v. 318, p. 330–333, doi:10.1038/318330a0.
- Williams, M.L., Jercinovic, M.J., Harlov, D.E., Budzyń, B., and Hetherington, C.J., 2011, Resetting monazite ages during fluid-related alteration: *Chemical Geology*, v. 283, no. 3-4, p. 218–225, doi:10.1016/j.chemgeo.2011.01.019.
- Zimmerman, U., Luna Tula, G., Marchioli, A., Narvaez, G., Olima, H., and Ramirez, A., 2002, Analisis de procedencia de la Formación Falda Cienaga (Ordovícico Medio, Puna Argentina) por petrografía sedimentaria, elementos trazas e isotopia de Nd: *Revista de la Asociación Argentina de Sedimentología*, v. 9, no. 2, p. 165–188.

SCIENCE EDITOR: DAVID I. SCHOFIELD  
ASSOCIATE EDITOR: WENJIAO XIAO

MANUSCRIPT RECEIVED 26 JULY 2016  
REVISED MANUSCRIPT RECEIVED 25 JANUARY 2017  
MANUSCRIPT ACCEPTED 25 APRIL 2017

Printed in the USA